Influence of the $N^*(1440)$ and $N^\star(1535)$ Resonances in Intermediate Energy pp and np Scattering

A. Pricking[(a,b)], Ch. Elster[(c)], A. Gårdestig[(d)], F. Hinterberger[(a)]
and the EDDA Collaboration
[(a)] *Helmholtz Institut für Strahlen- und Kernphysik, University of Bonn, Nussallee 14-16, D-53115 Bonn, Germany*
[(b)] *Physikalisches Institut der Universität Tübingen, D-72076 Tübingen, Germany*
[(c)] *Institute of Nuclear and Particle Physics, and Department of Physics and Astronomy, Ohio University, Athens, OH 45701, USA and*
[(d)] *Department of Physics and Astronomy, University of South Carolina, Columbia, SC 29208, USA*
(Dated: February 1, 2008)

Motivated by a recent measurement of proton-proton elastic scattering observables up to 3.0 GeV, we investigate the description of those data within models of the nucleon-nucleon (NN) interaction valid above the pion production threshold. In addition to including the well known Delta resonance we incorporate two low-lying N^* resonances, the $N^*(1440)$ and the $N^*(1535)$, and study their influence on pp and np observables for projectile laboratory kinetic energies up to 1.5 GeV.

PACS numbers: 13.75.Cs,25.40.Cm
Keywords:

I. INTRODUCTION

Elastic nucleon-nucleon (NN) scattering is a process fundamental to our understanding of the nuclear forces. This knowledge forms the basis for a broad range of applications from few-nucleon reactions to heavy ion physics. Consequently, many experimental and theoretical studies have been devoted to the subject. Since the measurements at, e.g., LAMPF [1, 2], the database has doubled, and global phase shift analyses now extend to 3.0 GeV projectile kinetic energy for pp scattering and 1.3 GeV for np scattering [3, 4]. Measurements of polarization observables (analyzing power, spin correlation coefficients, depolarization parameters and spin transfer triple coefficients) at discrete kinetic energies up to 2.9 GeV were obtained by the NNSaturne II Collaboration [5, 6]. At lower kinetic energies (0.2 - 0.45 GeV), precise analyzing powers and spin correlation coefficients have been provided by the PINTEX Collaboration [7–9] using the IUCF Cooler Ring and an internal polarized hydrogen target. At higher kinetic energies (0.45 - 2.5 GeV), precise and internally consistent excitation functions, i.e., differential cross sections [10, 11], analyzing powers [12, 13] and spin correlation parameters [14, 15], have recently been measured by the EDDA Collaboration using the Cooler Synchrotron COSY and internal targets. These new proton-proton elastic scattering data are included in the new global phase shift analysis up to 3.0 GeV kinetic energy with its most recent solution SP07 [3].

The theoretical description of the nuclear force also has quite a long history. During the last decade a lot of effort has been directed toward deriving the nuclear force in the framework of effective field theory (EFT), especially in the form of chiral perturbation theory (χPT). This EFT can be regarded as the low-energy limit of the underlying theory quantum chromodynamics (QCD) and inherits its spontaneously broken chiral symmetry. As first pointed out by Weinberg [16, 17], the nucleon-nucleon potential can be expanded in powers of the χPT expansion parameter $P \equiv \frac{p,m_\pi}{\Lambda_\chi}$, where $p \sim m_\pi$ is a typical nucleon three-momentum and $\Lambda_\chi \sim 1$ GeV is the chiral scale. Weinberg's idea has since been extended to several orders in the chiral expansion with NN potentials of χPT derived to NNLO in Refs. [18–20] and to N^{3}LO [21, 22]. At N^{3}LO the description of NN data below $E_{\rm lab} = 200$ MeV is comparable in quality to that obtained in the so–called "high-precision" NN potential models [23–25], provided cutoffs in the range 500–600 MeV are considered [22]. However, the energy range appropriate for the χPT expansion is determined by the expansion parameter P being "small". Thus energy regimes of ~ 0.5 GeV and higher are not accessible by currently employed EFT methods.

In the later 1980's and early 1990's considerable theoretical effort was directed towards understanding the NN interaction in the energy region between 0.4 and 1.0 GeV, which is dominated by the Delta isobar. These approaches may roughly be divided into two classes [26]. Firstly, there are the models based on a formulation of genuine unitary ($NN\pi$) three-particle equations, explicitly including the πN scattering amplitudes P_{33} [Delta (Δ) resonance] and P_{11} (Roper resonance) and usually employing separable potentials. The second approach is based on the extension of conventional low-energy potentials into the single-pion production region [27–30]. Most of these are based on coupled channel calculations containing NN, $N\Delta$ and $\Delta\Delta$ channels, and the single pion production is incorporated through the decay of the Delta isobar doorway states. The main differences between the two types of models are the choice of kinematics, the description of the width of the Delta resonance, and the choice of NN potential being extrapolated.

More recent theoretical work on the NN interaction in the energy domain around 0.5 GeV and higher was driven by the need of a better understanding of pion production in different reactions, e.g., in pion photoproduction from the deuteron in the Delta region [31, 32] and pion production in heavy-ion reactions [33], measured at GSI. The exploratory study of Ref. [34] investigates how well a meson exchange model containing the Delta resonance together with a Wood-Saxon type optical potential can describe cross sections and polarization observables in the region between 1 and 3 GeV. The authors point out that the polarization observables in pp scattering for energies above 1 GeV are badly represented by the model employed.

In this work we want to concentrate on the structure of the nuclear force as revealed in NN scattering between 1 and 1.5 GeV projectile kinetic energy, the so-called 2nd resonance region. This regime is dominated by low lying, well-isolated nucleon resonances. A better understanding of the properties and parameters of those resonances is now being pursued at Excited Baryon Analysis Center (EBAC) [35] based on photoproduction data at ELSA (Bonn), JLab (Newport News), MAMI (Mainz), GRAAL (Grenoble), and Spring-8 (Hyogo). We want to study the influence of the lowest lying πN resonances on the NN data in the region around 1 GeV, which is slightly beyond the region dominated by the Delta resonance. We start from a meson exchange model and introduce the lowest order loop diagrams containing the Δ, Roper, and S_{11} resonances into the model. In Section II we give the underlying interaction Lagrangians and in Section III we describe the resonance part of the potential and the parameterization of their width. In Section IV we describe our data fitting procedure, and in Section V we discuss our results obtained when successively introducing the resonances into the potential model. We summarize and conclude in Section VI.

II. RELATIVISTIC MESON-EXCHANGE MODEL FOR NN SCATTERING ABOVE THE PION THRESHOLD

For projectile energies in the GeV range it is mandatory to employ a relativistic formulation of NN scattering. A suitable starting point would be the four-dimensional Bethe-Salpeter equation [36], which however is very difficult to solve. The only successful solution for NN scattering including Delta isobar (Δ) degrees of freedom was obtained in Ref. [28]. Since three-dimensional scattering equations are more amenable for computations, so-called three-dimensional reductions of the Bethe-Salpeter equation have been used [29]. In this work we will use the reduction proposed by Thompson [37], which was also used in Ref. [34]. For completeness we give the invariant scattering amplitude $\hat{T}$ as introduced by the Thompson reduction:

$$\hat{T}(\mathbf{p}',\mathbf{p},W) = \hat{V}(\mathbf{p}',\mathbf{p}) + \int d\mathbf{k}\, \hat{V}(\mathbf{p}',\mathbf{k}) \frac{M^2}{E_k^2} \frac{1}{W+i\varepsilon-2E_k} \hat{T}(\mathbf{k},\mathbf{p},W). \tag{2.1}$$

Here W is the invariant mass of the NN system, $W = 2E_p$, and $E_p = \sqrt{p^2+M^2}$ in the c.m. system. Redefining the scattering amplitude as well as the potential as

$$T(\mathbf{p}',\mathbf{p},W) = \frac{M}{E_{p'}} \hat{T}(\mathbf{p}',\mathbf{p},W) \frac{M}{E_p}, \tag{2.2}$$

$$V(\mathbf{p}',\mathbf{p}) = \frac{M}{E_{p'}} \hat{V}(\mathbf{p}',\mathbf{p}) \frac{M}{E_p}, \tag{2.3}$$

leads to a scattering equation which has the form of a standard Lippmann-Schwinger equation with relativistic kinetic energies

$$T(\mathbf{p}',\mathbf{p},W) = V(\mathbf{p}',\mathbf{p}) + \int d\mathbf{k}\, V(\mathbf{p}',\mathbf{k}) \frac{1}{W+i\varepsilon-2E_k} T(\mathbf{k},\mathbf{p},W), \tag{2.4}$$

which can be solved with standard numerical techniques.

The pseudoscalar pion provides the long-range part of the nuclear force and most of the tensor forces. Shorter range contributions of the potential are being represented by the exchange of heavier mesons, the vector mesons ρ and ω, representing the 2π P-wave resonance and a 3π resonance. The ω provides most of the short range repulsion of the nuclear force. The intermediate attraction is provided by the exchange of a light scalar-isoscalar "σ"-meson, which has not been directly observed. A recent reanalysis [38] of $\pi\pi$ data gave evidence for the existence of a very broad resonance at threshold with the quantum numbers of the vacuum, a mass of about 440 MeV, and a width of about 272 MeV. For a simple model which still can capture basic features of the NN interaction the exchange of π (138 MeV), "σ" ($\simeq$ 500 MeV), ρ (769 MeV), and ω (783 MeV) is sufficient. The coupling of these mesons to the

nucleon is given by the following interaction Lagrangians

$$\mathcal{L}_{pv} = -\frac{f_{ps}}{m_{ps}}\bar{\psi}\gamma^5\gamma^\mu\psi\partial_\mu\varphi^{(ps)}, \tag{2.5}$$

$$\mathcal{L}_{s} = -g_s\bar{\psi}\psi\varphi^{(s)}, \tag{2.6}$$

$$\mathcal{L}_{v} = -g_v\bar{\psi}\gamma^\mu\psi\varphi^{(v)}_\nu - \frac{f_v}{4M}\bar{\psi}\sigma^{\mu\nu}\psi(\partial_\mu\varphi^{(v)}_\nu - \partial_\nu\varphi^{(v)}_\mu). \tag{2.7}$$

Here M is the nucleon mass, and m_α, with $\alpha = pv, ps, s, v$, denotes the masses of mesons with pseudo-vector, pseudo-scalar, scalar and vector character. If the mesons carry isospin, the field $\varphi^{(\alpha)}$ should be replaced by $\boldsymbol{\tau}\cdot\boldsymbol{\varphi}^{(\alpha)}$, where τ^i are the usual Pauli spin matrices. Very often one-boson-exchange (OBE) models also include the η (547 MeV) and the a_0 (980 MeV) [39]. However, if the scalar-isovector a_0 is included, there is no reason to not also consider the scalar-isoscalar f_0 (980 MeV) with similar mass, as well as the η' (958 MeV). It is clear that mesons with large masses will contribute to the short range part of the NN interaction. Thus their effect is very small when considering low energies, and there they can in principle be omitted. However, since we want to investigate a meson exchange model at laboratory energies around 1 GeV and higher, we include for consistency all strangeness-zero mesons with masses below 1 GeV.

In order to introduce contributions from the nucleon resonances into the potential model, we consider the lowest order loop diagrams containing a resonance as an intermediate state. The first diagrams to consider are those with a nucleon and a single resonance (Δ, P_{11}, S_{11}) in the intermediate state. As a first step we want to consider here only low lying S- and P-wave resonances. These resonances can be on-shell at the NN laboratory kinetic energies $T_{\rm lab} = 632$ MeV for the $N\Delta$, 1136 MeV for the NP_{11}, and 1381 MeV for the NS_{11} diagrams, respectively. These energies are given in Table I together with the pion and eta production thresholds. The energy at which two Delta's are on shell in an intermediate state is below the threshold for the NS_{11} intermediate state, therefore the diagram with $\Delta\Delta$ intermediate states is also included in our calculation. The diagrams included are shown in Fig. 1.

Since the Delta is an isospin-3/2 state, only isovector mesons can excite it. The only possible exchange mesons are then π and ρ. Note that in order to fulfill the weak unitarity bound ($\sigma_{\rm tot} > \sigma_{\rm el}$), diagrams with π-π, π-ρ, and ρ-ρ exchange must all be included. The P_{11} resonance has the quantum numbers of the nucleon and decays predominantly into $N\pi$ (60-70%) [40] and to a lesser extent to $N\pi\pi$. We consider here the exchange of a pion and in addition the exchange of a "σ", which mimics (correlated) two-pion exchanges. The decay of the P_{11} into $N\rho$ has a probability of less than 8% and thus this ρ exchange is not considered. The S_{11} resonance is the only known resonance that couples strongly to the $N\eta$ channels. The dominant decay channels are $N\pi$ and $N\eta$ [40]. Thus, for this resonance we consider only the exchange of π and η. Again, in order to fulfill the weak unitarity bound, each of the diagrams in Fig. 1 represents in reality four separate diagrams.

The interaction Lagrangians for the couplings to the Delta are given by

$$\mathcal{L}_{N\Delta\pi} = -\frac{f_{N\Delta\pi}}{m_\pi}\bar{\psi}\mathbf{T}\psi^\mu\partial_\mu\varphi^{(\pi)} + \text{H.c.} \tag{2.8}$$

$$\mathcal{L}_{N\Delta\rho} = -i\frac{f_{N\Delta\rho}}{m_\rho}\bar{\psi}\gamma^5\gamma^\mu\mathbf{T}\psi^\nu\left(\partial_\mu\varphi^{(\rho)}_\nu - \partial_\nu\varphi^{(\rho)}_\mu\right) + \text{H.c.}, \tag{2.9}$$

where ψ_μ is the Rarita-Schwinger field [41–43] describing the spin-3/2 Delta-isobar and ψ stands for the nucleon field. The operator $\mathbf{T}$ acts between isospin-1/2 and isospin-3/2 states and H.c. denotes the Hermitian conjugate.

The P_{11} resonance has the quantum numbers of the nucleon with the interaction Lagrangians given by

$$\mathcal{L}_{NN^*_{P_{11}}\pi} = -\frac{f_{NN^*_{P_{11}}\pi}}{m_\pi}\,\bar{\psi}_{P_{11}}\gamma^5\tau\psi\partial_\mu\varphi_\pi + \text{H.c.}, \tag{2.10}$$

$$\mathcal{L}_{NN^*_{P_{11}}\sigma} = -g_{NN^*_{P_{11}}\sigma}\,\bar{\psi}_{P_{11}}\psi\varphi_\sigma + \text{H.c.} \tag{2.11}$$

In contrast to the P_{11} resonance, the S_{11} resonance has negative parity, and the interaction Lagrangians are given by [44]

$$\mathcal{L}_{NN^*_{S_{11}}\pi} = -ig_{NN^*_{S_{11}}\pi}\,\bar{\psi}_{S_{11}}\tau\,\psi\varphi_\pi + \text{H.c.}, \tag{2.12}$$

$$\mathcal{L}_{NN^*_{S_{11}}\eta} = -ig_{NN^*_{S_{11}}\eta}\,\bar{\psi}_{S_{11}}\psi\varphi_\eta + \text{H.c.} \tag{2.13}$$

All the meson-baryon vertices described by the above Lagrangian interactions are modified by form factors of the dipole-type

$$F_\alpha\left((\mathbf{p}'-\mathbf{p})^2\right) = \left(\frac{\Lambda_\alpha^2 - m_\alpha^2}{\Lambda_\alpha^2 + (\mathbf{p}'-\mathbf{p})^2}\right)^{n_\alpha}, \tag{2.14}$$

where $(\mathbf{p}' - \mathbf{p})$ is the momentum transfer between the two interacting baryons. The parameter Λ_α is the so-called cutoff mass and is determined by fitting NN data. We choose $n_\alpha = 1$ for all vertices with the exception of the $N\Delta\rho$ vertex, where $n_\alpha = 2$ is applied.

III. RESONANCE CONTRIBUTIONS TO THE POTENTIAL

The nucleon resonances enter the NN potential via the loop diagrams given in Fig. 1. Schematically, the contribution to the potential from these "iterative" diagrams can be written as

$$V_{NN,R_1R_2}\ \frac{1}{W - E_{R_1} - E_{R_2}}\ V_{R_1R_2,NN}. \tag{3.1}$$

Here W is the invariant mass of the NN system, and E_{R_1}, E_{R_2} the energies $E_{R_i} = \sqrt{m_{R_i}^2 + k^2}$ of the intermediate states, which can be either a nucleon, a $\Delta(1232)$, a $N^*(1440)$ or a $N^*(1535)$. The transition potentials $V^\pi_{NN,N\Delta}$ and $V^\pi_{NN,\Delta\Delta}$ can be found in Ref. [45] and $V^\rho_{NN,N\Delta}$ and $V^\rho_{NN,\Delta\Delta}$ in Ref. [46]. The transition potentials for the two N^* resonances can be calculated in a straightforward fashion, since they carry isospin 1/2. Since the resonances have a finite life time, their mass is modified by the width of the resonance according to

$$\mu_{r_i} = m_{r_i} - i\frac{\Gamma_{r_i}}{2}. \tag{3.2}$$

Because of the finite width Γ_{r_i}, the mass, and thus the energy of the resonances, acquires an imaginary contribution. The loop diagrams of Fig. 1 then contain an imaginary piece, which describes the inelasticity of the NN scattering process above the pion threshold. The effect of direct pion production in NN scattering up to 1 GeV has been studied in Refs. [28, 47], and found to be very small in comparison to pion production via, e.g., the Δ-resonance. For the present purpose π (and η) production will be restricted to occur only via resonance doorway states.

We follow here the same parameterization of the penetrability as given in Ref. [33], i.e.,

$$\Gamma = \gamma q v_L(qR). \tag{3.3}$$

Here the momentum q is the c.m. momentum of the πN system [or ηN system in case of the $N^*(1535)$], and should not be confused with the momenta in the NN system. The parameter R is fitted and chosen such that the product qR becomes dimensionless. We choose $R = 6.3$ GeV^{-1} for all three resonances under consideration. The dimensionless quantity γ is the reduced width, and the penetrability factor v_L is defined as

$$v_L(qR) = \frac{1}{(qR)^2 n_L^2(qR) + (qR)^2 j_L^2(qR)}, \tag{3.4}$$

where L denotes the orbital angular momentum quantum number of the resonance. The functions j_L and n_L are the spherical Bessel and Neumann functions. Thus for the resonances Δ and $N^*(1440)$ with the quantum numbers of P_{33} and P_{11} the width is given as

$$\Gamma_{\Delta,P_{11}} = \gamma_{\Delta,P_{11}} \frac{q^3R^2}{1 + q^2R^2}\ \Theta(q - q_{thr}) \tag{3.5}$$

and for the resonance $N^*(1535)$ with the quantum numbers S_{11}

$$\Gamma_{S_{11}} = \gamma_{S_{11}} q\ \Theta(q - q_{thr}), \tag{3.6}$$

where the step function $\Theta(q - q_{thr})$ ensures that the pion (eta) production starts at the corresponding thresholds in the NN c.m. frame. The expressions for Γ_{r_i} show that the resonance width increases linearly with increasing momentum q and introduces a linear divergence in the imaginary part of the potential. Since this does not seem physical plausible, Ref. [33] introduced an additional phenomenological form factor to the resonance width of the form

$$Z(q^2) = \frac{q^2(m_{r_i}^2) + \kappa^2}{q^2(s) + \kappa^2}, \tag{3.7}$$

so that Eq. (3.3) is modified to

$$\Gamma = \gamma q v_L(qR)\ Z(q^2). \tag{3.8}$$

As already mentioned in Ref. [33], the analytic form of the form factor is relatively unimportant, as long as the resonance curve is qualitatively described, i.e., it peaks at the resonance position. However, at the energies we are considering, setting $Z(q^2) = 1$ has only minor influence on the numerical calculation of the NN observables. Even so, we choose to employ Eq. (3.7) for the physical reason already mentioned. The form factor is defined such that it is 1 at the exact resonance position, $s = m_{r_i}^2$, of the meson-nucleon system. The parameters γ_{r_i} are fitted such that the resonance width at the resonance position coincides with the experimentally extracted width [40]. A similar behavior has been observed in Ref. [30] where the resonance width is calculated as the imaginary part of the lowest order $\Delta N\pi$ loop diagram. There a dipole cutoff with the same cutoff parameter $\Lambda_{N\Delta\pi}$ as employed in the NN potential was used.

Since we consider only single π (or η) production, we fit the width Γ_{r_i} to the corresponding partial widths as given in Ref. [40]. However, the Δ resonance decays with a probability $> 99\%$ into $N\pi$. Thus, in this case the partial width is equal to the total width, which lies between 115 and 125 MeV. For the $N^*(1440)$ resonance we use the partial width for the $N\pi$ decay to determine the strength parameters. The total width has a wide ranging from 200 MeV to 450 MeV Ref. [40]. We choose the value $\Gamma_{P_{11}}^{\rm tot} = 391$ MeV, from Ref. [48] to determine the partial width.

The $N^*(1535)$ resonance decays mostly into $N\pi$ and $N\eta$. Up to the η-production threshold, which corresponds to the NN laboratory energy 1253 MeV, we only consider the partial width for $N\pi$ decay, above the η threshold we add also the partial width for the $N\eta$ decay. The parameters we use for describing the width of the resonances included in our model are given in Table II. We tested the influence of the width cutoff parameter κ on the NN observables. Varying κ between about 200 and 1000 MeV did not lead to any visible difference in their description. Thus, for the Δ resonance we used the value (200 MeV) given in Ref. [33], while we for the two N^* resonances we adopted an average value of 400 MeV.

IV. FITTING PROCEDURE

The parameters in our model are the masses of the mesons and baryons, together with the coupling constant and cutoff parameters for the baryon-baryon-meson vertices. With one exception the masses are fixed to the values recommended by the Particle Data Group (PDG) [40]. For the nucleon mass we employ the average of the neutron and proton mass, $M = 938.926$ MeV. Similarly, for the pion mass we use the average of the charged and neutral pion masses. The only mass parameters which are not fixed are those of the "σ" mesons (one for each isospin channel), which we consider as free parameters. Since most meson-baryon coupling constants are poorly known, we treat them as free parameters, which are allowed to vary within a certain range. We use the values of Refs. [30, 49] as starting points. The only exception is the $NN\pi$ coupling, which we fixed to $g_{NN\pi}^2/4\pi = 13.8$, according to recent measurements at IUCF [50] and extractions by the Nijmegen group [51]. All cutoff parameters Λ are treated as free parameters and we allowed them to vary between 0.8 and 2.5 GeV. A more detailed discussion of the parameters obtained in the different fits will be given in the next section.

Our goal is to find parameter sets for which our models give a good description of the NN observables, i.e., total and differential cross sections, as well as spin observables, up to 1.5 GeV. However, we do not fit directly to data but rather to a partial wave analysis, since in some cases the amount of data is rather sparse. As reference values we choose the SAID energy dependent phase shift solution Sp07 from the CNS Data Analysis Center [52]. However, we need to prepare from this solution a "data set" that is suitable for our fitting procedure. First, since the imaginary parts of our model are already fixed by fitting the widths of the resonances to their experimental values (see Section III), the partial wave inelasticities ρ_l are already given. Therefore, we need to restrict ourselves to fitting only the phase shifts δ_l. Also, since we keep the pion coupling constant $g_{NN\pi}^2$ fixed, we should not include higher partial waves in the fit. What constitutes a high partial wave is expected to depend on the energy considered. Therefore, we divide the energy range up to 1.5 GeV into three separate regions: up to 0.3 GeV laboratory kinetic energy we include only partial waves $J \leq 2$ as reference values, between 0.3 and 0.8 GeV we consider all partial waves with $J \leq 4$, and above 0.8 GeV we include in addition all partial waves with $J \leq 6$. However, since there are only very few experimental data points for *np* scattering above 0.8 GeV, we exclude isospin-0 partial waves from the SAID data base above 0.8 GeV.

In addition we need to account for the fact that the SAID energy-dependent solutions do not give errors. The absolute errors for each partial wave are estimated with a simple polynomial reflecting the errors of the single energy solution. In this way we try to account for the accuracy of the phase shift analysis, which varies with energy and partial waves due to different amount of available data. Especially partial waves with small absolute values get a very large relative error assigned, since they would be overrepresented if only simple relative errors were used. However, in order to avoid obscuring the plots, these errors are not included in our figures. In all cases, the assigned errors increase monotonically with energy and reach a maximum absolute value of 2 at 1.5 GeV. We tested different error setups and choose the one giving the best overall results. All partial waves get similar errors assigned. However additional weight-factors could be included during the fitting procedure itself, e.g. the $^3P_2$ partial wave above 800 MeV was

assigned a low weight in the final fits. After creating our "data base" according to these specifications, we perform a nonlinear least-square fit using the Minuit program provided by the CERN library [53]. A discussion of the resulting model parameters and the description of the phase shifts and observables will be given in the following section.

The resonances are added one-by-one to our model, starting form a traditional meson-exchange NN scattering model. This way the influence of the different resonances can be understood separately from each other.

V. RESULTS AND DISCUSSION

A. Including the $\Delta(1232)$ – P_{33} Resonance

As a first step we consider only a meson exchange model together with the excitations of the $\Delta(1232)$ resonance. This is similar to the models used in Ref. [34, 49]. Here our focus is to create an updated model to which we can later add the P_{11} and S_{11} resonances. Thus, we first concentrate on the description of NN data up to 1 GeV, the energy regime which is expected to be dominated by the $\Delta(1232)$ resonance. In addition we include the contributions of the mesons a_0, f_0, and η', which all have a mass slightly below 1 GeV and were not included in [34, 49]. The influence these mesons have on the description of the phase shifts is relatively small and the coupling constants are determined to be of the order unity by our fitting procedure. They were allowed to vary within the interval [0.0,5.0] and the fit always stayed within these boundaries.

The ρ-meson tensor-to-vector coupling ratio was allowed to vary within the limits of 5.9 and 6.3. The fit prefers a value of 5.9, to which the ratio was kept fixed in the subsequent investigations. In the case of the ω meson this ratio is around -0.12 and of negligibly small influence. We thus fixed it to zero. We also studied the interplay between η and η' by alternately fixing one and letting the other one float. It turns out that, for the description of the NN phase shifts, only the combined strength of the two seem to matter, i.e., if one is fixed larger (on the order of 5) the other one will go to a smaller value, closer to 1. Therefore we always choose similar starting values for both of them, and let them vary between 1 and 6. Both couplings stayed within this range. Quark model prediction [54] give slightly higher values, but do predict both of them to be of the same magnitude. For the "σ" meson we let the coupling constants, masses, and cutoffs vary separately in the $T = 1$ and $T = 0$ channels. However, the values for the masses always stayed relatively close together.

Finally, we investigated the sensitivity of the $\Delta(1232)$ couplings to the overall description of the phase shifts. In [34, 49] the value of $f^2_{N\Delta\pi}/4\pi = 0.35$ is used. Similarly, the πN model from Ref. [55] employs $f^2_{N\Delta\pi}/4\pi = 0.36$. On the other hand, quark models relating $f^2_{N\Delta\pi}$ to $f^2_{NN\Delta\pi}$ lead to values as low as 0.22 [56]. Because of this discrepancy we let the $f^2_{N\Delta\pi}$ float between those two values to see if the phase shifts show a preference. In addition we also let the cutoff $\Lambda_{N\Delta\pi}$ vary. The fit always prefers the lower value of the coupling constant and goes to the lower limit of the cutoff boundary, which was set for all couplings to 800 MeV. After lowering that bound even further, the cutoff $\Lambda_{N\Delta\pi}$ stabilizes at values between 600 and 700 MeV. Our fit runs consistently prefer a small value of $f^2_{N\Delta\pi}$, so we fixed this coupling for all further studies to 0.224. Since we independently fitted the width of the Δ resonance to its experimental value, this choice of coupling constant does not influence the size of the inelasticity provided by the $N\Delta\pi$ contribution. A similar investigation of the $f^2_{N\Delta\rho}$ coupling did not reveal any sensitivity with respect to the NN phase shifts. Thus we kept the value for $f^2_{N\Delta\rho}/4\pi$ the same as in Refs. [34, 49] and only varied the cutoff parameter $\Lambda_{N\Delta\rho}$.

In total we varied 22 parameters in this model, which includes the $\Delta(1232)$ resonance as the only means for pion production. It is well known that models of this kind are able to describe NN scattering up to about 1 GeV in semi-quantitative terms. A good parameter set obtained from our fit procedure is given as model (A) in Table III. Using those parameters we calculated pp and np observables as function of the projectile laboratory kinetic energy. The total cross section for elastic and inelastic pp scattering are shown in Fig. 3 as a long-dashed line together with the SAID Sp07 analysis [4]. As already pointed out in Ref. [34], the inelastic contributions of a model of this type are not large enough to account for the experimentally observed ones. Consequently the total elastic cross section is being overpredicted beyond 1 GeV. This tendency can also be observed in the differential cross section for pp scattering in Fig. 4, especially at the larger angles. A partial remedy would be double pion production, which starts to contribute above 590 MeV. We will not attempt to include such amplitudes in the present paper. The differential cross section for np scattering (Fig. 5) is experimentally less well determined than for pp and data above 800 MeV are sparse. Overprediction of the np differential cross section is only visible at the largest c.m. angle.

The analyzing power A_N is shown in Fig. 6 for pp and in Fig. 7 for np scattering. Above about 800 MeV the analyzing power for pp scattering is strongly overpredicted, especially for the larger angles. This phenomenon was already pointed out in Ref. [34]. The np analyzing power is also overpredicted at similar angles, however at angles larger than 90° our calculation describes the existing data quite well. The spin correlation coefficients A_{SS}, A_{NN}, and A_{LL} for different c.m. angles are shown as function of projectile kinetic energy in Figs. 8–10 for pp scattering and

in Fig. 11 for np scattering. For the spin-correlation coefficient A_{SS} the model predictions deviate from the data in a similar way as for the analyzing power, whereas the other spin-correlation coefficients are described reasonably well.

In addition to the energy dependence of observables (for fixed angles) we also select three different fixed energies for c.m. angular distributions of pp observables. Those energies are 400 MeV (Fig. 12), 800 MeV (Fig. 13), and 1300 MeV (Fig. 14). As can be expected from the previous discussion, at 400 MeV our calculations are in reasonable agreement with the data, while deviations start to show up at 800 MeV and become more severe at 1300 MeV.

The partial wave phase shifts of our model prediction (A) up to J=4 are shown as long-dashed lines in Fig. 15 ($T = 1$) and Fig. 16 ($T = 0$). The imaginary parts of the partial wave amplitudes are given in Fig. 17 ($T = 1$) and Fig. 18 ($T = 0$).

B. Including the $N^*(1440)$ – P_{11} Resonance

The $N^*(1440)$ (Roper) resonance is the lowest $J = \frac{1}{2}$ nucleon excitation and thus the first nucleon resonance to add. Since it has the same quantum numbers as the nucleon this resonance couples to exactly the same meson fields as the nucleon, though not necessarily with the same strength. We are using the decay modes of the Roper as guide to which meson exchanges to include. It decays predominantly into the $N\pi$ channel (60-70%) [40]. A very crude estimate from the width of the Roper resonance indicates that the $NN^*\pi$ coupling is about 40% of the $NN\pi$ coupling. In Ref. [57], Riska and Brown extract an average $f^2_{NN^*\pi}/4\pi = 0.0012$ from the width and derive an even smaller quark model estimate. On the other hand, a coupled channel model for πN scattering [55] uses $f^2_{NN^*\pi}/4\pi = 0.0024$. We choose a value close to the latter, since the overall effect of the iterative $NN^*(1440)$ diagram is quite small. The second largest decay channel of the Roper is $N\Delta\pi$ (20-30%) and PDG gives a value of 5-10% for $N(\pi\pi)_{\rm s-wave}$. To mimic the latter effect, at least for the real part of the amplitudes, we introduce the "σ" meson, and choose a relatively small value for its coupling. During the fitting procedure this value stayed small and none of our fits reached the large value favored in Ref. [55]. The calculations in Ref. [33] introduced additional diagrams containing ρ and ω exchange in the iterative $NN^*(1440)$ diagram, though with relatively small coupling constants. As a test we included the ω meson, but since the overall effect in phase shifts and observables is minimal, we did not pursue the inclusion of vector mesons any further.

Adding the $N^*(1440)$ resonance to model (A), without refitting the parameters, has only a moderate effect on both the $T = 1$ and $T = 0$ phase shifts. However, to obtain a true assessment of the effect, the model parameters need to be readjusted. A qualitative fit to the phase shift including the $N^*(1440)$ resonance is given by the parameters listed in Table IV. The results are plotted as short dashed lines in Figs. 3–18.

A major effect of the $N^*(1440)$ can be seen in the $T = 0$ channels, which now exhibit pion production at threshold. Since $N\Delta$ contributions are forbidden, pion production close to threshold is provided solely by the decay of the Roper resonance. Overall, the total cross section for inelastic scattering is slightly increased. However, the contributions of the $N^*(1440)$ are by far too small to make up the difference with the experimental data. Though the changes in the $^1P_1$ and $^3P_2$ phase shifts are relatively large in going from model (A) to model (B), the final differences in the observables are much smaller.

Thus, the inclusion of the Roper resonance has a small overall effect in the description of NN scattering. However, it is vital for the $T = 0$ inelasticities close to threshold. Similar conclusions were drawn in Ref. [27]. We see in our fit that the pion-nucleon cutoff is slightly reduced when the Roper resonance is included. Thus we were tempted to see if we can force $\Lambda_{NN\pi}$ to take a small value, e.g., 1 GeV, and still obtain a description of the data of equal quality by letting the $NN^*\pi$ coupling take arbitrary values. In fact, it has been suggested [58] that a soft $NN^*\pi$ form factor can be used in a boson-exchange model provided an additional pseudoscalar meson, with a mass slightly above 1 GeV, is introduced. We find, however, that despite the Roper resonance having the quantum numbers of the nucleon, the iterative NN^* diagram with pion exchanges can not assume this particular role, and we can not get acceptable fits with a very soft pion form factor.

C. Including the $N^*(1535)$ – S_{11} Resonance

The $N^*(1535)$ (S_{11}) resonance has the quantum numbers of the nucleon, except it is parity-odd. Thus the functional forms of the vertices have different spin structures, see Eqs. (2.12) and (2.13). The $N^*(1535)$ decays mainly into the $N\pi$ and $N\eta$ channels, and thus we include only these mesons when considering the iterative diagram with the S_{11} resonance in the intermediate state. Values for the coupling $g^2_{NN^*\pi}/4\pi$ vary considerably in the literature. The quark model estimate from Riska and Brown [57] suggests that it is slightly less then half of the $NN\pi$ coupling, while investigations of πN scattering give a value as low as 0.001 [59]. A study of η photoproduction from the deuteron [60] suggests a value of 0.1. Our value of 0.05 obtained from the fit is well within these boundaries. The NN data are

not particularly sensitive to this number as long as it stays around 0.1. For the coupling to the η meson we obtained 0.99, which is higher than the value of 0.33 given in Refs. [59, 60].

When including the $N^*(1535)$ resonance (without refitting), its effect is most prominent in the $^1\mathrm{P}_1$ phase shift. In general, the $T = 0$ phase shifts are more sensitive to the size of its contribution. However, a true assessment should only be made after a refit of the parameters. This gives the parameters of Table V, which constitute our model (C). The observables calculated with these parameters are plotted in Figs. 3–14, partial wave phase shifts in Figs. 15 and 16, and the imaginary parts of the scattering amplitudes in Figs. 17 and 18 (solid lines in all figures).

In general, the $N^*(1535)$ resonance has a tendency to counterbalance the contributions of the $N^*(1440)$ resonance. A description of NN observables with both N^* resonances is of about the same quality as the description containing only the Δ resonance. Only a closer look at the inelasticities in the np phase shifts shows that these two resonances are necessary in order to obtain inelastic contributions in the region close to threshold.

Comparing the parameters of model (C), given in Table V, with the parameters of the other two models shows that the coupling of the ω meson decreases when introducing the $N^*(1535)$ resonance, indicating that this contribution has an overall repulsive effect. The ρ coupling, on the other hand, decreases minimally. In addition, the pion cutoff, $\Lambda_{NN\pi}$, assumes a slightly lower value.

D. Role of the $^3P_2$ Partial Wave in the Description of Polarization above 800 MeV

Certain observables are particularly sensitive to specific phase shifts. For example, the analyzing power A_N is sensitive to spin-triplet states. Above roughly 800 MeV the analyzing power is strongly overpredicted for larger c.m. angles, as seen in Fig. 6 for the pp excitation function. This effect is also seen in the corresponding np analyzing power, however not as strongly. Thus, one needs to concentrate on the large discrepancies seen in the $T = 1$ triplet phase shifts. The most obvious candidate is the $^3\mathrm{P}_2$ phase shift, which above 800 MeV deviates strongly from the experimental analysis. The experimental analysis changes sign at about 1 GeV, while the model predictions remain positive and roughly constant.

In order to isolate the influence of the $^3\mathrm{P}_2$ partial wave on the observables, especially on the analyzing power, we replaced the phase-shift $\delta(^3\mathrm{P}_2)$ from our model above 800 MeV with the one from the SAID analysis and then recalculated the observables. Since the inelasticity agrees with the SAID analysis, we stayed with our model prediction for this parameter. The resulting pp differential cross section and analyzing power are shown as function of laboratory kinetic energy for c.m. angles 33° and 53° in Fig. 19, together with the original prediction for comparison. The large discrepancy almost completely vanishes. In Fig. 20 the differential cross section and analyzing power at 800 and 1300 MeV are shown as function of c.m. scattering angle. Again, once the $^3\mathrm{P}_2$ partial wave is replaced with the SAID value, the discrepancy nearly disappears. All the other observables are only marginally affected by this change in the $^3\mathrm{P}_2$ partial wave. The description of the analyzing power for np scattering at 53°, Fig. 7, is also improved by the change in the $^3\mathrm{P}_2$ partial wave, while the backward angles are not affected and remain reasonably well described. For higher energies, the pp analyzing power is a smooth function of the energy at nearly all angles [4]. Thus we may speculate that once the fast change of sign of the $^3\mathrm{P}_2$ partial wave between 800 and 1500 MeV wave is explained, the pp analyzing power can be described reasonably well. However, the present ingredients in our model can not account for a correct description of the $^3\mathrm{P}_2$ partial wave. The efforts of Ref. [34] indicate that a variation of model parameters close to our model (A) is not able to improve the description of the analyzing power as function of energy. Instead, a different physical mechanism needs to come into play. A strong energy dependence in one single partial wave often indicates the opening of a new threshold in that particular channel, given by the coupling to another nucleon resonance. Since the $^3\mathrm{P}_2$ partial wave has a very strong energy dependence above 800 MeV one may speculate that only a S-wave coupling to this partial wave can be responsible, which would require a $J = \frac{5}{2}$ resonance. The lowest $J = \frac{5}{2}$ resonances have masses around 1.7 GeV and were found to be important for a description of πN scattering below 2 GeV [35, 61]. Consideration of either the $\mathrm{D}_{15}(1675)$ or the $\mathrm{F}_{15}(1680)$ would be possible candidates to explore this avenue.

VI. SUMMARY AND CONCLUSIONS

In this paper we have studied the effects the first few resonances have on the description of the NN phase shifts in the energy regime around and above 1 GeV. We have incorporated the $\Delta(1232)$ resonance as well as the $N^*(1440)$ and $N^*(1535)$ in a relativistic meson-exchange model. We started with a model including contributions of only the $\Delta(1232)$ resonance, which we refitted to NN data up to 1 GeV, and then added the contributions of the $N^*(1440)$ and $N^*(1535)$ resonances, now extending the fitted region up to 1.5 GeV. We verified the characteristic deficiencies in describing the pp analyzing powers above ∼800 MeV that were pointed out already in Ref. [34]. We could isolate this

defect as being caused by a poor description of the $^3P_2$ partial wave above 800 MeV. This situation is not improved by including also the two N^* resonances. We speculate that only a new channel, which couples with $L = 0$ to the $^3P_2$ partial wave will be able to cause such a strong energy dependence in that specific partial wave. Further investigations are necessary to investigate this assertion.

We also find that, in general, the description of available *np* observables seems to be better than that of *pp* observables. However, this finding may be too optimistic due to the small amount of *np* observables above 1 GeV. We also observe that the total cross section for inelastic scattering is underpredicted by about a factor of two by our models, indicating that not enough inelastic channels are considered. In Ref. [34] this was compensated for by introducing a spin-independent optical potential providing an average absorption. As shown there, this provides a reasonable mechanism to incorporate a bulk contribution to account for single- and multiple-meson production. However, such an optical potential will not be able to account for the strong energy dependence in selected partial waves, e.g., the $^3P_2$ partial wave around 1 GeV.

In this work the main effort was introducing contributions of two of the lowest N^* resonances into the description of NN observables above 1 GeV laboratory kinetic energy. In order to have uniform description of the widths of the resonances we employ the relatively simple parameterization suggested in Ref. [33]. This can be improved by taking advantage of the recent work of the Excited Baryon Analysis Center (EBAC) [35] analyzing πN scattering in region below the 2 GeV nucleon resonance region, and e.g. employing vertex functions and self-energies determined in the πN analysis in the NN system. This will allow to make connections between analyses of electromagnetic meson production reactions and the understanding of the NN system in this energy regime.

Acknowledgments

This work was performed in part under the auspices of the U. S. Department of Energy under contract No. DE-FG02-93ER40756 with Ohio University and the German BMBF under contract No. 06BN664I(6). It was also supported by the U. S. National Science Foundation grant PHY-0457014. Helpful discussions and the support of Heiko Rohdjess is gratefully acknowledged. The authors thank W. J. Briscoe and I. I. Strakovsky for making the files of Sp07 available for use in this manuscript. One of the authors (Ch.E.) acknowledges inspiring discussions with T.-S.H. Lee and the hospitality of the ANL Theory Group during the final stages of the manuscript.

[1] M. W. McNaughton *et al.*, Phys. Rev. **C23**, 1128 (1981); *ibid* **C24**, 1778 (1981); *ibid* **C25**, 1967 (1982).
[2] R. A. Arndt *et al.*, Phys. Rev. **D28**, 97 (1983).
[3] R. A. Arndt, W. J. Briscoe, I. I. Strakovsky and R. L. Workman, [arXiv:nucl-th/0706.2195].
[4] The full SAID database can be accessed at *http://gwdac.phys.gwu.edu*.
[5] NNSaturne II Collaboration (J. Ball *et al.*), *Proton-proton Data Measured by the Nucleon-nucleon Collaboration at Saturne II*, CTU Rep. **4**, 3 (2000).
[6] C. E. Allgower *et al.*, Nucl. Phys. **A637**, 231 (1998); Eur. Phys. J. **C5**, 453 (1998); Phys. Rev. C **64**, 034003 (2001).
[7] PINTEX Collaboration (W. Haeberli *et al.*), Phys. Rev. C **55**, 597 (1997).
[8] PINTEX Collaboration (B. Przewoski *et al.*), Phys. Rev. C **58**, 1897 (1998).
[9] PINTEX Collaboration (F. Rathmann *et al.*), Phys. Rev. C **58**, 658 (1998).
[10] EDDA Collaboration (D. Albers *et al.*), Phys. Rev. Lett. **78**, 1652 (1997).
[11] EDDA Collaboration (D. Albers *et al.*), Eur. Phys. J. A **22**, 125 (2004).
[12] EDDA Collaboration (M. Altmeier *et al.*), Phys. Rev. Lett. **85**, 1819 (2000).
[13] EDDA Collaboration (M. Altmeier *et al.*), Eur. Phys. J. A **23**, 351 (2005).
[14] EDDA Collaboration (F. Bauer *et al.*), Phys. Rev. Lett. **90**, 142301 (2003).
[15] EDDA Collaboration (F. Bauer *et al.*), Phys. Rev. C **71**, 054002 (2005).
[16] S. Weinberg, Phys. Lett. B **251**, 288 (1990).
[17] S. Weinberg, Nucl. Phys. B **363**, 3 (1991).
[18] C. Ordonez, L. Ray, and U. van Kolck, Phys. Rev. C **53**, 2086 (1996.
[19] N. Kaiser, R. Brockmann, and W. Weise, Nucl. Phys. A **625**, 758 (1997) [arXiv:nucl-th/9706045].
[20] E. Epelbaum, W. Glöckle, and U.-G. Meißner, Nucl. Phys. A **671**, 295 (2000).
[21] E. Epelbaum, W. Glöckle, and U.-G. Meißner, Nucl. Phys. A **747**, 362 (2005).
[22] D. R. Entem and R. Machleidt, Phys. Rev. C **68**, 041001 (2003).
[23] R. B. Wiringa, V. G. J. Stoks, and R. Schiavilla, Phys. Rev. C **51**, 38-51 (1995).
[24] V. G. J. Stoks, R. A. M. Klomp, C. P. F. Terheggen, and J. J. de Swart, Phys. Rev. C **49**, 2950 (1994).
[25] R. Machleidt, Phys. Rev. C **63**, 024001 (2001).
[26] For reviews see Ch. Elster, Nucl. Phys. **A508**, 197c (1990); H. H. Garzilazo and T. Mizutani, Few-Body Systems **5**, 127 (1988).

[27] M. Betz and T.-S. H. Lee, Phys. Rev. **C23**, 375 (1981); T.-S. H. Lee, Phys. Rev. **C29**, 195 (1984); T.-S. H. Lee and A. Matsuyama, Phys. Rev. **C36**, 1459 (1987).
[28] E. E. van Faassen and J. A. Tjon, Phys. Rev. **C33**, 2105 (1986).
[29] E. E. van Faassen and J. A. Tjon, Phys. Rev. **C30**, 285 (1984); **C28**, 2354 (1983).
[30] Ch. Elster, K. Holinde, D. Schütte, and R. Machleidt, Phys. Rev. C**38**, 1828 (1988).
[31] M. Schwamb and H. Arenhövel, Nucl. Phys. **A690**, 647 (2001).
[32] A. Matsuyama, T. Sato, and T.-S. H. Lee, Phys. Rep. **439**, 193 (2007).
[33] S. Huber and J. Aichelin, Nucl. Phys. **A573**, 587 (1994).
[34] K. O. Eyser, R. Machleidt, and W. Scobel, Eur. Phys. J. **A22**, 105 (2004).
[35] B. Julia-Diaz, T. S. Lee, A. Matsuyama and T. Sato, [arXiv:nucl-th/0704.1615].
[36] E. E. Salpeter and H. A. Bethe, Phys. Rev. **84**, 1232 (1951).
[37] R. H. Thompson, Phys. Rev. **D1**, 110 (1970).
[38] I. Caprini, G. Colangelo, and H. Leutwyler, Phys. Rev. Lett. **96**, 132001 (2006).
[39] R. Machleidt, K. Holinde, and Ch. Elster, Phys. Rep. **149**, 1 (1987).
[40] Particle Data Group, W.-M. Yao *et al.*, J. Phys. G**33**, 1 (2006).
[41] W. Rarita and J. Schwinger, Phys. Rev. **60**, 61 (1941).
[42] D. Luriè, *Particles and Fields*, Interscience, New York, 1968.
[43] O. Dumbrajs, R. Koch, H. Pilkuhn, G. C. Oades, H. Behrens, J. J. de Swart, and P. Kroll, Nucl. Phys. **B216**, 277 (1983).
[44] M. Benmerrouche and N. C. Mukhopadhyay, Phys. Rev. Lett. **67**, 1070 (1991).
[45] K. Holinde and R. Machleidt, Nucl. Phys. **A280**, 429 (1977).
[46] K. Holinde, R. Machleidt, M. R. Anastasio, A. Faessler, and H. Müther, Phys. Rev. **C18**, 870 (1978).
[47] Ch. Elster, W. Ferchländer, K. Holinde, D. Schütte, and R. Machleidt, Phys. Rev. C**37**, 1647 (1988).
[48] D. M. Manley and E. M. Saleski, Phys. Rev. D **45**, 4002 (1992).
[49] Ch. Elster and P. C. Tandy, Phys. Rev. C **40**, 881 (1989).
[50] M. Sarsour *et al.*, Phys. Rev. Lett. **94**, 082303 (2005), Phys. Rev. C **74**, 044003 (2006).
[51] V. G. J. Stoks, R. Timmermans and J. J. de Swart, Phys. Rev. C **47**, 512 (1993).
[52] Center for Nuclear Studies (CNS) Data Analysis Center, *http://gwdac.phys.gwu.edu/*.
[53] SEAL Math Libraries Work Package, *seal.web.cern.ch/seal/work-packages/mathlibs/*.
[54] C. Downum, T. Barnes, J. R. Stone and E. S. Swanson, Phys. Lett. B **638**, 455 (2006).
[55] C. Schutz, J. Haidenbauer, J. Speth and J. W. Durso, Phys. Rev. C **57**, 1464 (1998).
[56] G. E. Brown and W. Weise, Phys. Rep. **22**, 279 (1975).
[57] D. O. Riska and G. E. Brown, Nucl. Phys. A **679**, 577 (2001).
[58] K. Holinde and A. W. Thomas, Phys. Rev. C **42**, R1195 (1990).
[59] O. Krehl, C. Hanhart, S. Krewald, and J. Speth, Phys. Rev. C **62**, 025207 (2000).
[60] E. Breitmoser and H. Arenhövel, Nucl. Phys. A **612**, 321 (1997).
[61] V. Shklyar, G. Penner and U. Mosel, Eur. Phys. J. A **21**, 445 (2004).

Threshold	$T_{\rm lab}$ [MeV]
$NN\pi$	285
$N\Delta$	632
$NN^*(1440)$	1136
$NN\eta$	1256
$\Delta\Delta$	1355
$NN^*(1535)$	1381

TABLE I: Laboratory (kinetic) energy thresholds for single-pion and single-eta production in the NN system. In case of the resonances, the number indicates the laboratory kinetic energy for which the resonance becomes on-shell.

Resonance	Channel	$\Gamma_{\rm partial}$ [MeV]	R [GeV^{-1}]	γ	κ [MeV]
Δ	$N\pi$	$\sim 120^{(a)}$	6.3	0.749	200
$N^*(1440)$	$N\pi$	$\sim 270^{(b)}$	6.3	0.75	400
$N^*(1535)$	$N\pi$	$\sim 60^{(a)}$	6.3	0.1286	400
$N^*(1535)$	$N\eta$	$\sim 79^{(a)}$	6.3	0.4284	400

TABLE II: The parameters for the description of the partial resonance width as given in Eq. (3.8). The superscript (a) indicates values taken from Ref. [40], (b) indicates the value from Ref. [48].

Vertex	α	J^P	I	m_α	$\frac{g^2_{NN\alpha}}{4\pi}$	f_α/g_α	Λ_α [MeV]
$NN\alpha$	π	0^-	1	138.03	13.8		1519
	η	0^-	0	547.3	5.81		830
	ρ	1^-	1	769.	1.1	5.9	1281
	ω	1^-	0	782.6	23.1	0.	1382
	$\sigma\ (T=1)$	0^+	0	497.	5.505		1807
	$\sigma\ (T=0)$	0^+	0	480.	3.545		1990
	a_0	0^+	1	980.	4.75		1004
	η'	0^-	0	958.	1.62		1433
	f_0	0^+	0	980.	2.5		1274
					$\frac{f^2_{N\Delta\alpha}}{4\pi}$		$\Lambda_{N\Delta\alpha}$ [MeV]
$N\Delta\alpha$	π	0^-	1	138.03	0.224		640
	ρ	1^-	1	769.	20.45		1508

TABLE III: Meson parameters of the model (A) including the Δ isobar as the only mechanism for pion production. J, P, and I denote spin, parity and isospin of the meson. Each meson vertex is multiplied by a form factor as given in Eq. (2.14), where n_α= 1 except for the $NN\rho$ vertex where n_α= 2.

Vertex	α	J^P	I	m_α	$\frac{g^2_{NN\alpha}}{4\pi}$	f_α/g_α	Λ_α [MeV]
$NN\alpha$	π	0^-	1	138.03	13.8		1498
	η	0^-	0	547.3	2.0		1300
	ρ	1^-	1	769.	1.1	5.9	1281
	ω	1^-	0	782.6	23.6	0.	1396
	σ $(T=1)$	0^+	0	494.	5.195		1924
	σ $(T=0)$	0^+	0	495.	3.603		1700
	a_0	0^+	1	980.	4.75		1004
	η'	0^-	0	958.	1.24		1433
	f_0	0^+	0	980.	2.5		1471
					$\frac{f^2_{N\Delta\alpha}}{4\pi}$		$\Lambda_{N\Delta\alpha}$ [MeV]
$N\Delta\alpha$	π	0^-	1	138.03	0.224		677
	ρ	1^-	1	769.	20.45		1508
					$\frac{f^2_{NN^*\pi}}{4\pi}$	$\frac{g^2_{NN^*\sigma}}{4\pi}$	$\Lambda_{NN^*\alpha}$ [MeV]
$NN^*(1440)\alpha$	π	0^-	1	138.03	0.023		800
	σ	0^+	1	494.		0.74	1119

TABLE IV: Meson parameters of the model (B) including Δ isobar and the $N^*(1440)$ as mechanism for pion production. J, P, and I denote spin, parity and isospin of the meson. Each meson vertex is multiplied with a form factor as given in Eq. (2.14), where n_α= 1 except for the $NN\rho$ vertex where n_α= 2.

Vertex	α	J^P	I	m_α	$\frac{g^2_{NN\alpha}}{4\pi}$	f_α/g_α	Λ_α [MeV]
$NN\alpha$	π	0^-	1	138.03	13.8		1429
	η	0^-	0	547.3	2.0		1298
	ρ	1^-	1	769.	0.97	5.9	1310
	ω	1^-	0	782.6	20.5	0.	1421
	σ $(T=1)$	0^+	0	503.	5.254		2000
	σ $(T=0)$	0^+	0	530.	4.164		1516
	a_0	0^+	1	980.	4.75		968
	η'	0^-	0	958.	1.57		1424
	f_0	0^+	0	980.	2.31		1442
					$\frac{f^2_{N\Delta\alpha}}{4\pi}$		$\Lambda_{N\Delta\alpha}$ [MeV]
$N\Delta\alpha$	π	0^-	1	138.03	0.224		618
	ρ	1^-	1	769.	20.45		1422
					$\frac{f^2_{NN^*\pi}}{4\pi}$	$\frac{g^2_{NN^*\sigma}}{4\pi}$	$\Lambda_{NN^*\alpha}$ [MeV]
$NN^*(1440)\alpha$	π	0^-	1	138.03	0.023		800
	σ	0^+	0	503.		0.74	1119
					$\frac{g^2_{NN^*\alpha}}{4\pi}$		$\Lambda_{NN^*\alpha}$ [MeV]
$NN^*(1535)\alpha$	π	0^-	1	138.03	0.05		809
	η	0^-	0	547.3.	0.99		962

TABLE V: Meson parameters of the model (C) including Δ isobar and the nucleon resonances $N^*(1440)$ and $N^*(1535)$ as mechanism for pion production. J, P, and I denote spin, parity and isospin of the meson. Each meson vertex is multiplied with a form factor as given in Eq. (2.14), where n_α= 1 except for the $NN\rho$ vertex where n_α= 2.

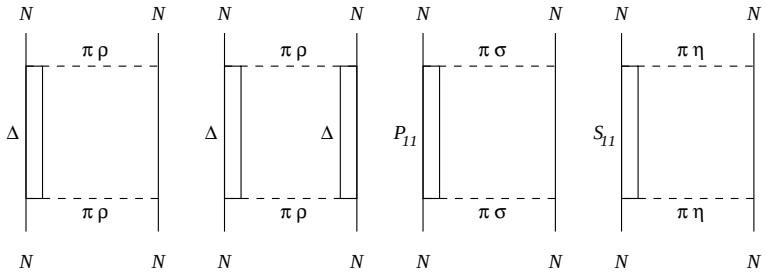

FIG. 1: The two-meson exchange iterative contributions involving nucleons (represented by solid lines) and nucleon resonances (double line). The dashed lines represent the exchanged mesons. The nucleon resonances and exchanged mesons are specified in the figure.

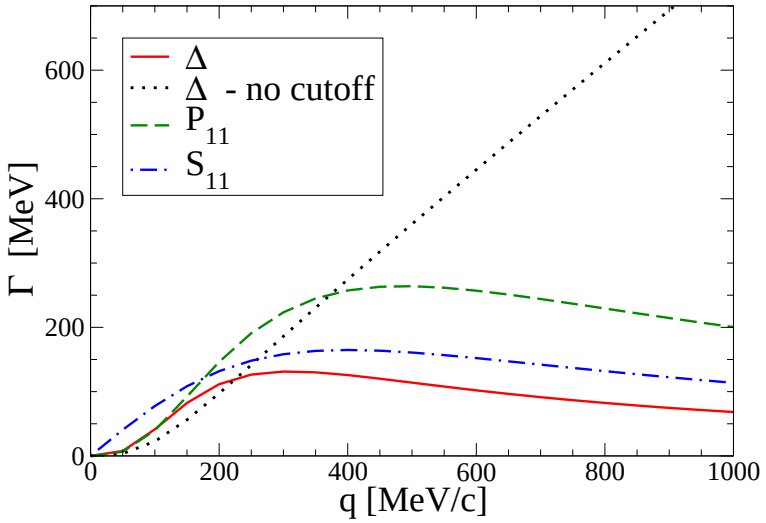

FIG. 2: The width of the resonances $\Delta(1232)$ (solid line), $N^*(1440)$ (dashed line) , and $N^*(1535)$ (dash-dotted line) as function of the c.m. momentum of the resonance. The dotted line indicates the width of the Δ resonance when no cutoff κ is applied.

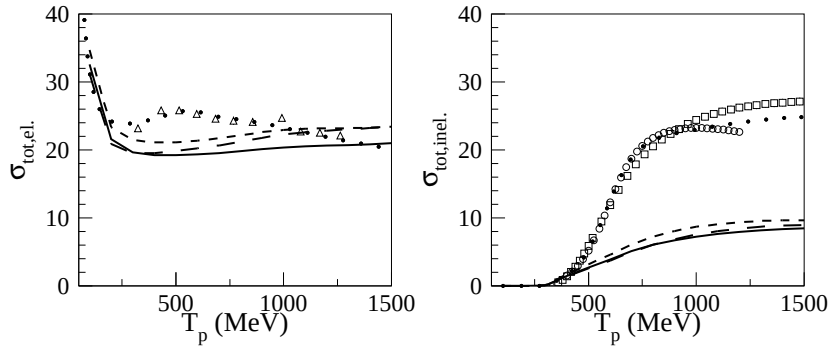

FIG. 3: The total cross section for elastic (left) and inelastic (right) *pp* scattering as function of the laboratory projectile kinetic energy. The solid line gives the prediction of the model C (Table V), containing the contributions of all three resonances P_{33}, P_{11}, and S_{11}. The short-dashed line is based on the model B (Table IV) containing only the resonances P_{33} and P_{11}. The long-dashed line represents the results of model A (Table III) containing only the P_{33} resonance in addition to the one-meson contributions. The SAID analysis Sp07 [3] is indicated by the dotted line. The experimental data are referenced in the SAID database [4].

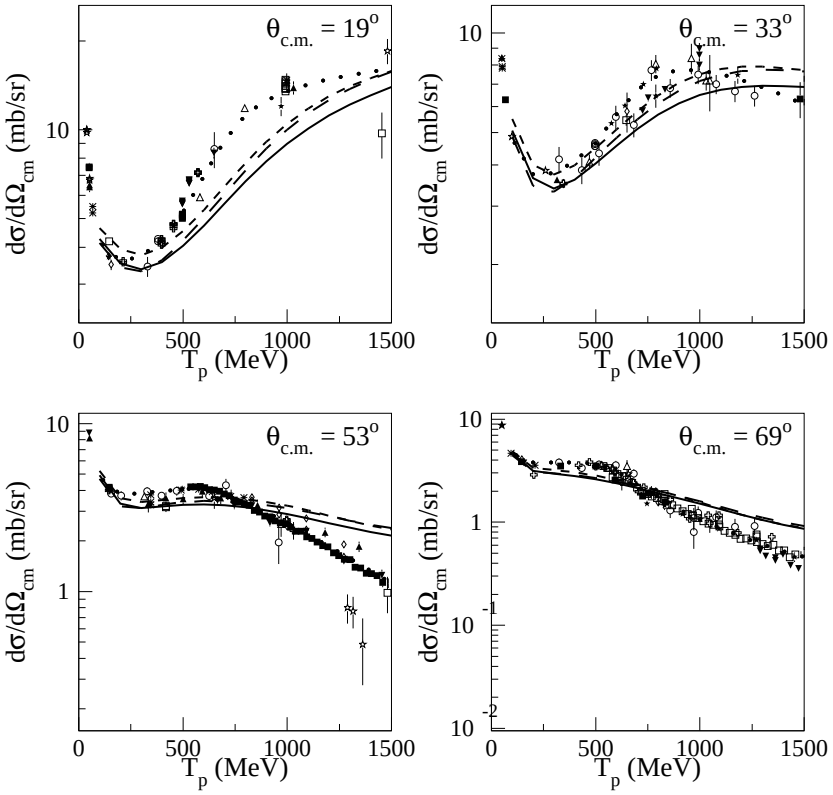

FIG. 4: The differential c.m. cross section for *pp* scattering as function of the laboratory projectile kinetic energy at selected angles. The notation of the curves is the same as in Fig. 3. The experimental data are referenced in the SAID database [4].

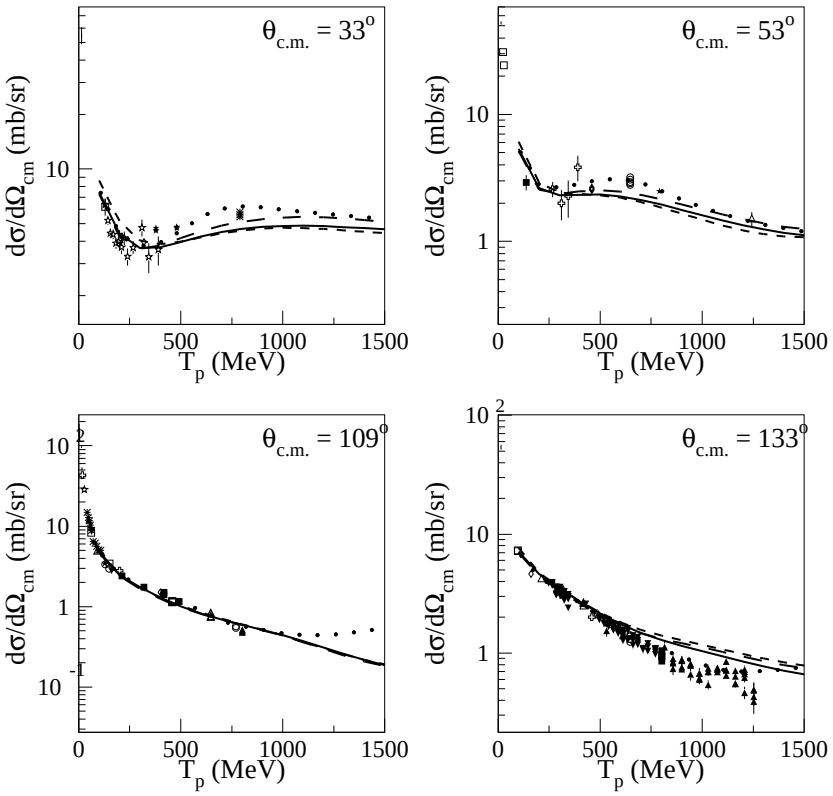

FIG. 5: The differential cross section for *np* scattering as function of the laboratory projectile kinetic energy at selected angles. The notation of the curves is the same as in Fig. 3. The experimental data are referenced in the SAID database [4].

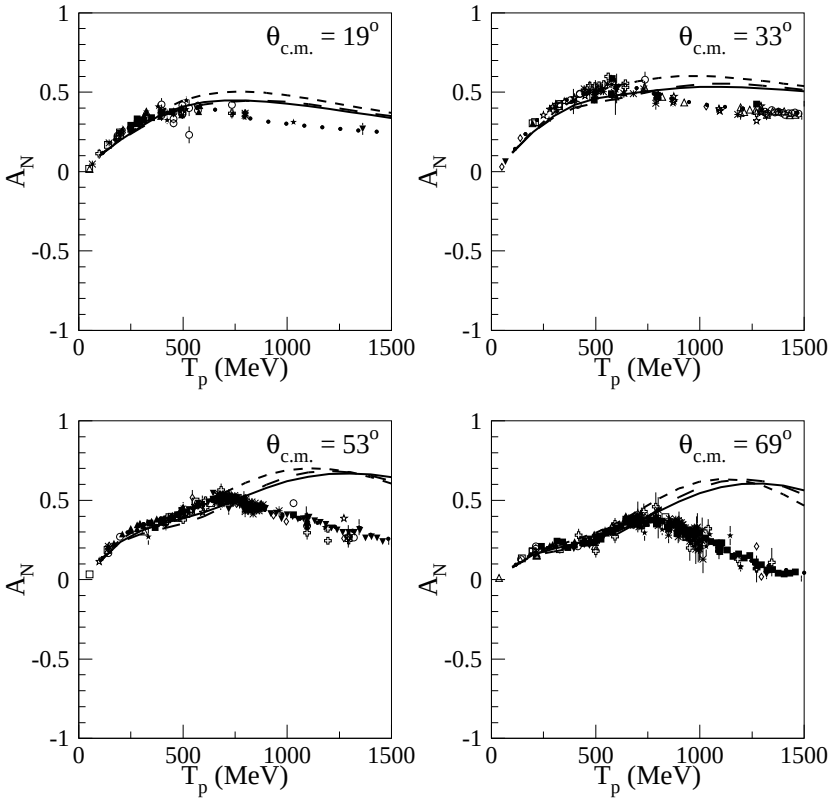

FIG. 6: The analyzing power A_N for pp scattering as function of the laboratory projectile kinetic energy at selected angles. The notation of the curves is the same as in Fig. 3. The experimental data are referenced in the SAID database [4].

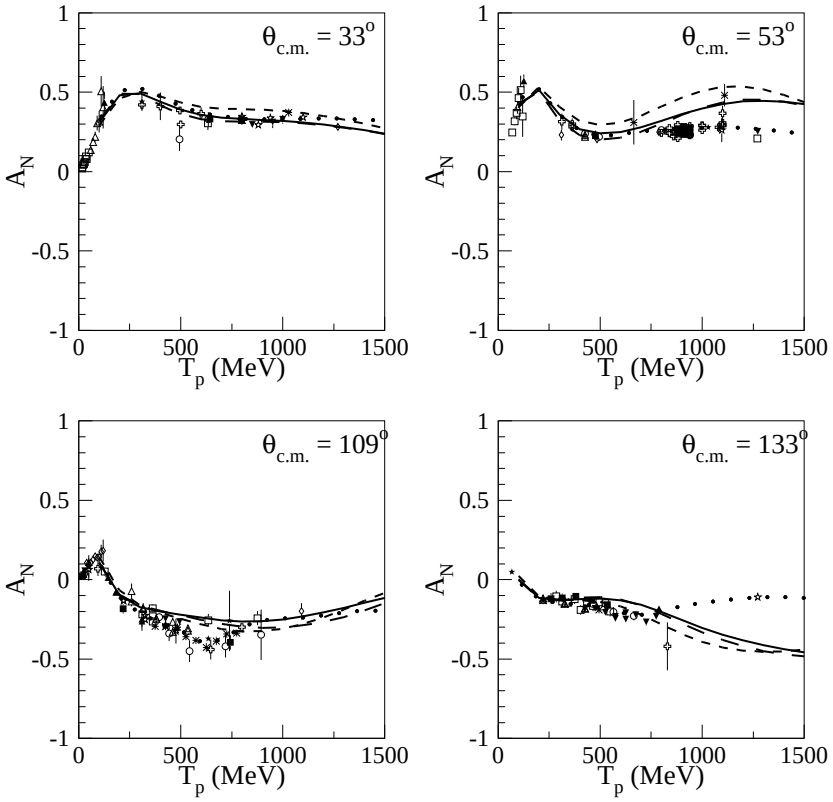

FIG. 7: The analyzing power A_N for np scattering as function of the laboratory projectile kinetic energy at selected angles. The notation of the curves is the same as in Fig. 3. The experimental data are referenced in the SAID database [4].

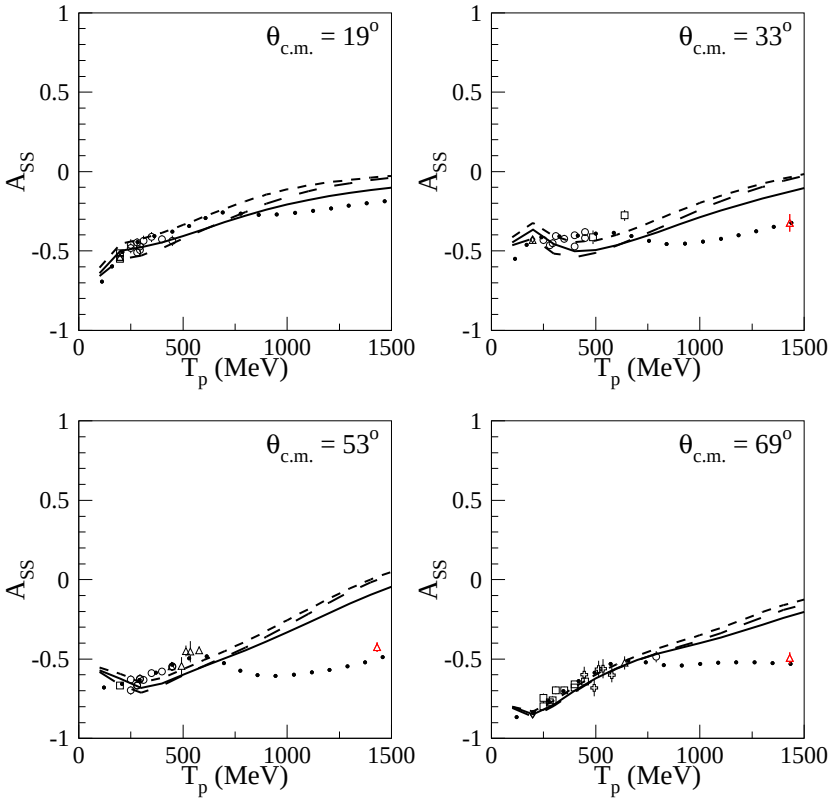

FIG. 8: The spin-correlation parameter A_{SS} for pp scattering as function of the laboratory projectile kinetic energy at selected angles. The notation of the curves is the same as in Fig. 3. The experimental data are referenced in the SAID database [4].

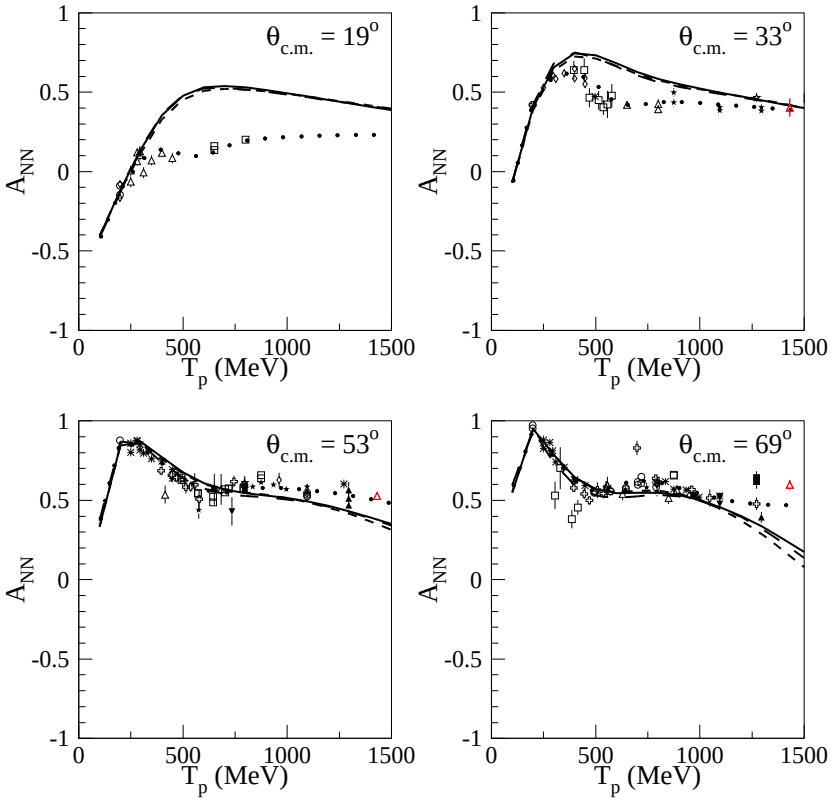

FIG. 9: The spin correlation parameter A_{NN} for *pp* scattering as function of the laboratory projectile kinetic energy at selected angles. The notation of the curves is the same as in Fig. 3. The experimental data are referenced in the SAID database [4].

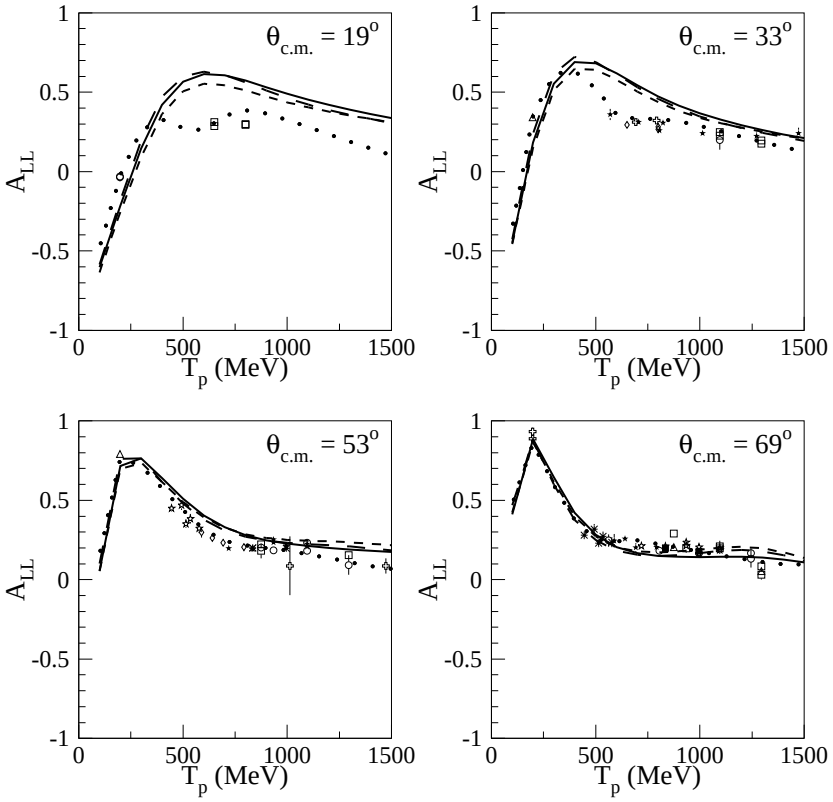

FIG. 10: The spin correlation parameter A_{LL} for *pp* scattering as function of the laboratory projectile kinetic energy at selected angles. The notation of the curves is the same as in Fig. 3. The experimental data are referenced in the SAID database [4].

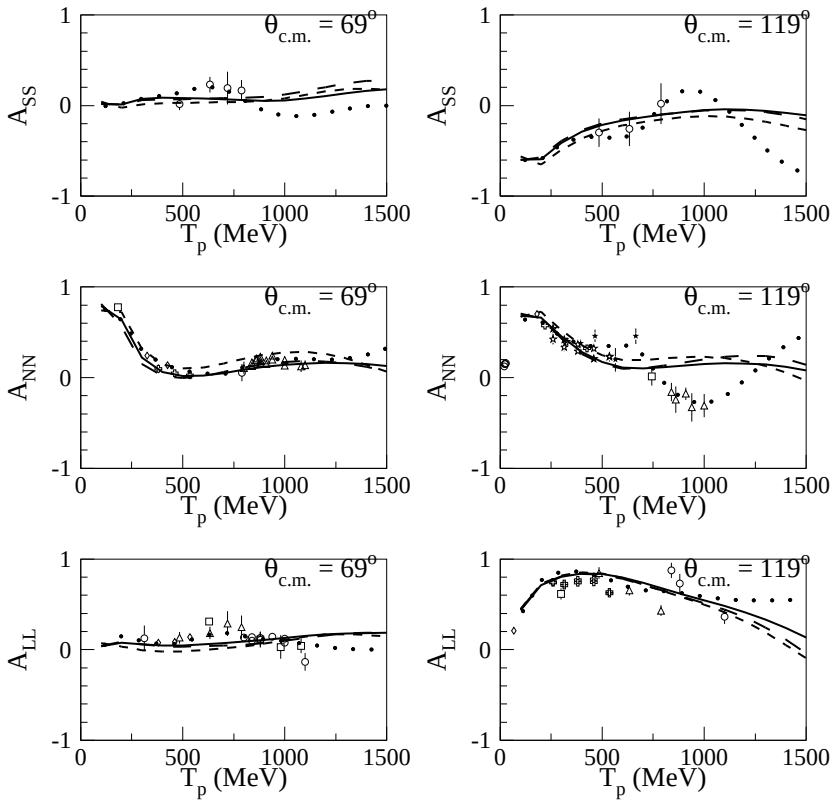

FIG. 11: The spin correlation parameters A_{SS}, A_{NN}, and A_{LL} for np scattering as function of the laboratory projectile kinetic energy at selected angles. The notation of the curves is the same as in Fig. 3. The experimental data are referenced in the SAID database [4].

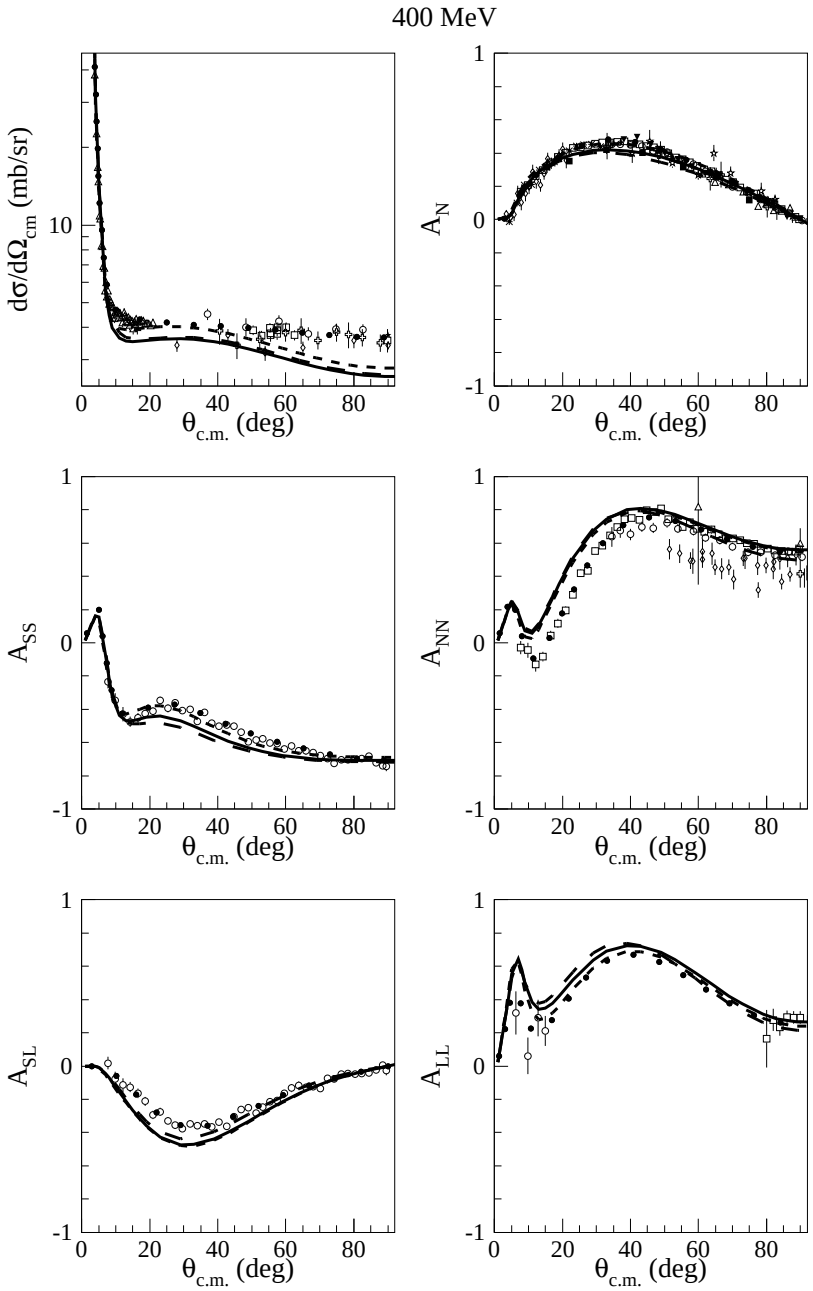

FIG. 12: The angular distribution of the differential cross section, the analyzing power and selected spin-correlation coefficients for *pp* scattering at 400 MeV laboratory kinetic energy. The notation of the curves is the same as in Fig. 3. The experimental data are referenced in the SAID database [4].

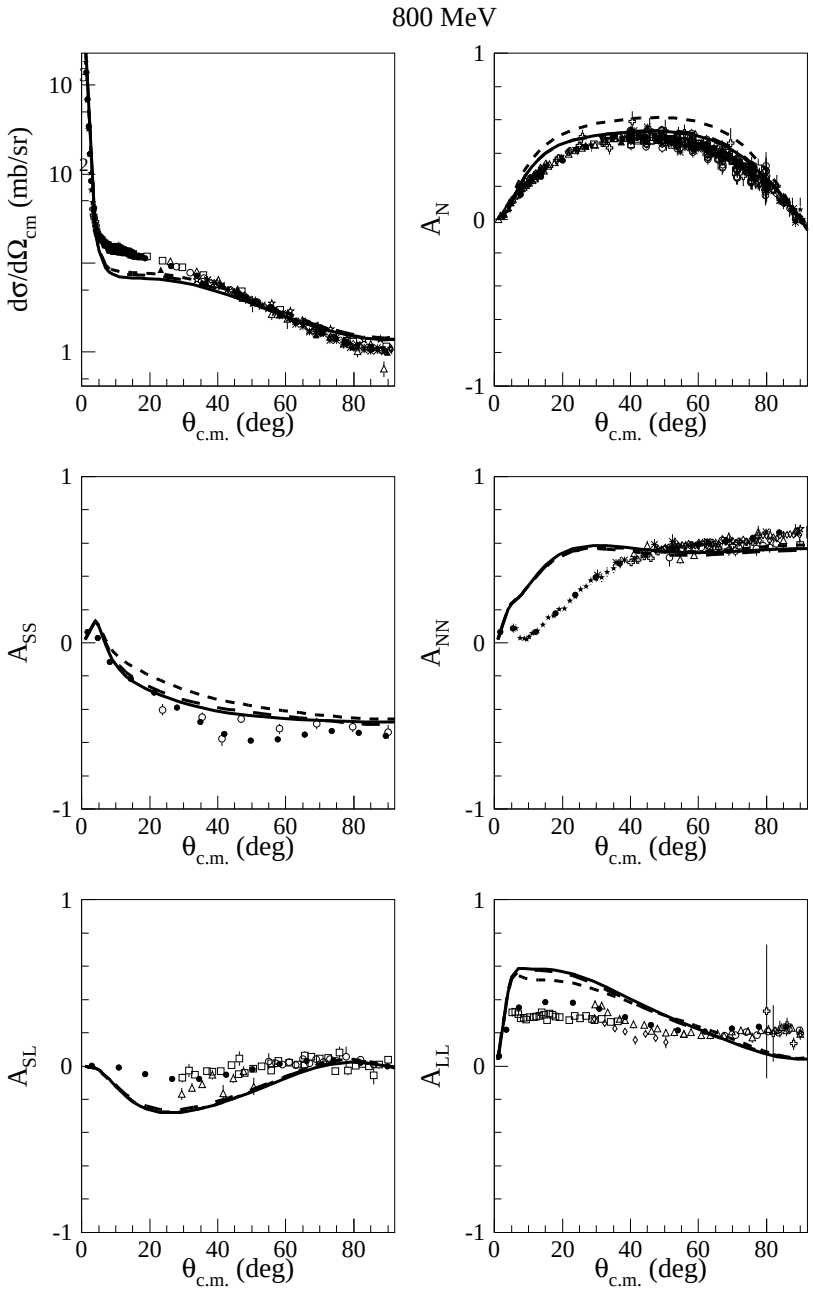

FIG. 13: The angular distribution of the differential cross section, the analyzing power and selected spin-correlation coefficients for *pp* scattering at 800 MeV laboratory kinetic energy. The notation of the curves is the same as in Fig. 3. The experimental data are referenced in the SAID database [4].

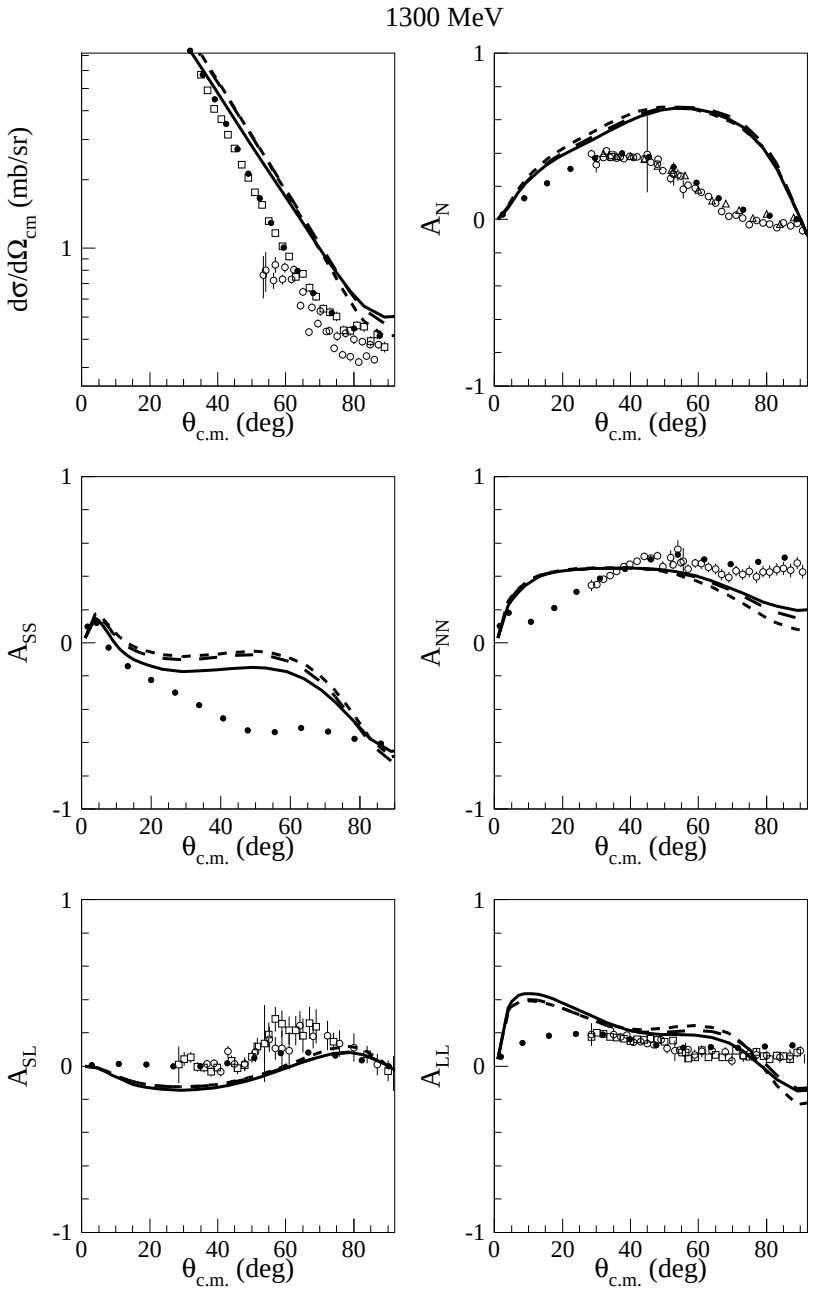

FIG. 14: The angular distribution of the differential cross section, the analyzing power and selected spin-correlation coefficients for *pp* scattering at 1300 MeV laboratory kinetic energy. The notation of the curves is the same as in Fig. 3. The experimental data are referenced in the SAID database [4].

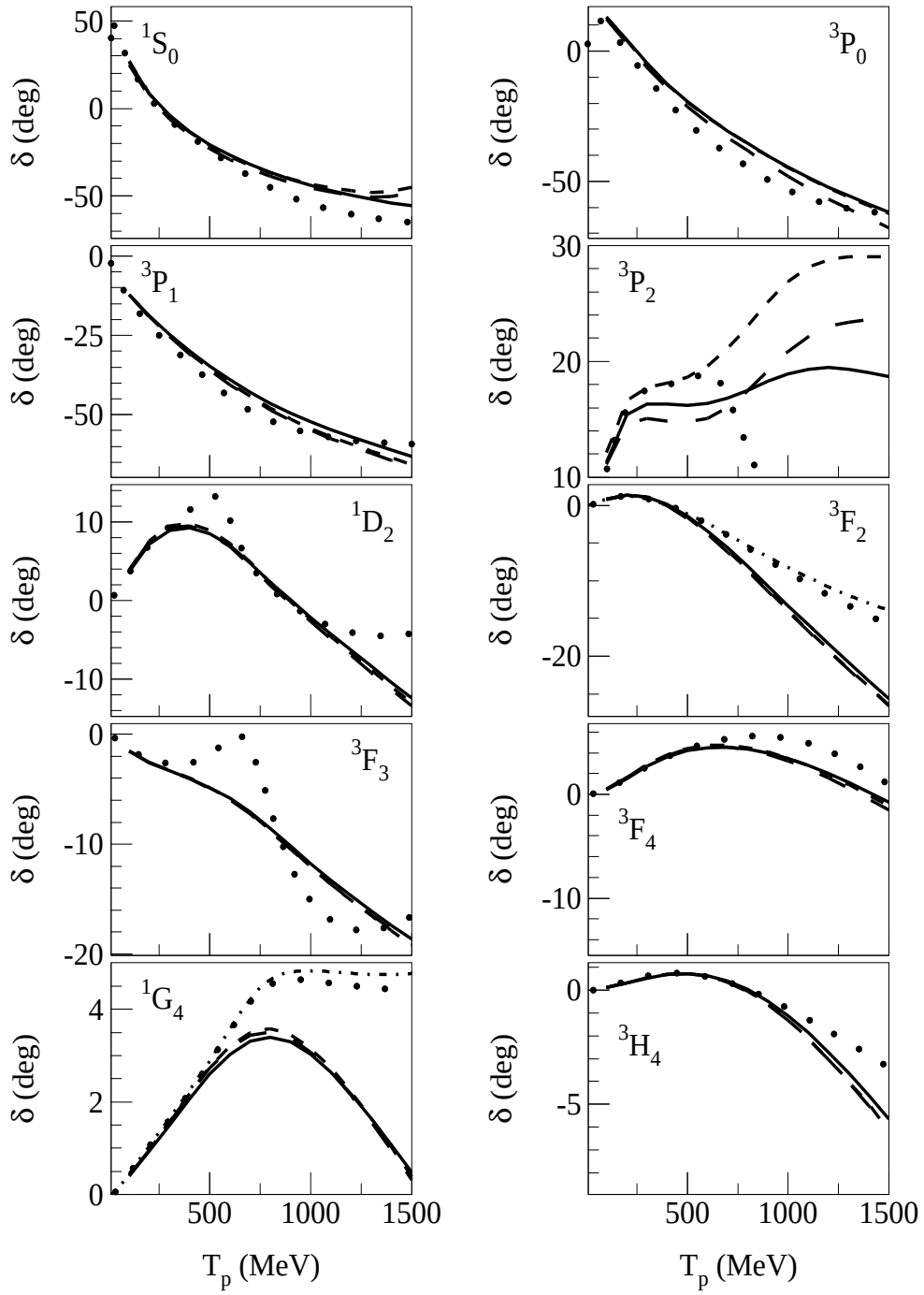

FIG. 15: The $T = 1$ NN partial wave phase shifts up to J=4 as function of the projectile laboratory kinetic energy. The solid line gives the prediction of the model C (Table V), containing the contributions of the resonances P_{33}, P_{11}, and S_{11}. The short-dashed line is based on the model B (Table IV) containing only the resonances P_{33} and P_{11}. The long-dashed line represents the results of model A (Table III) containing only the P_{33} resonance in addition to the one-meson contributions. The SAID analysis Sp07 [3] is indicated by the dotted line. The dash-dotted line in selected phase shifts (here $^3F_2$ and $^1G_4$) represents the SAID analysis Sp04.

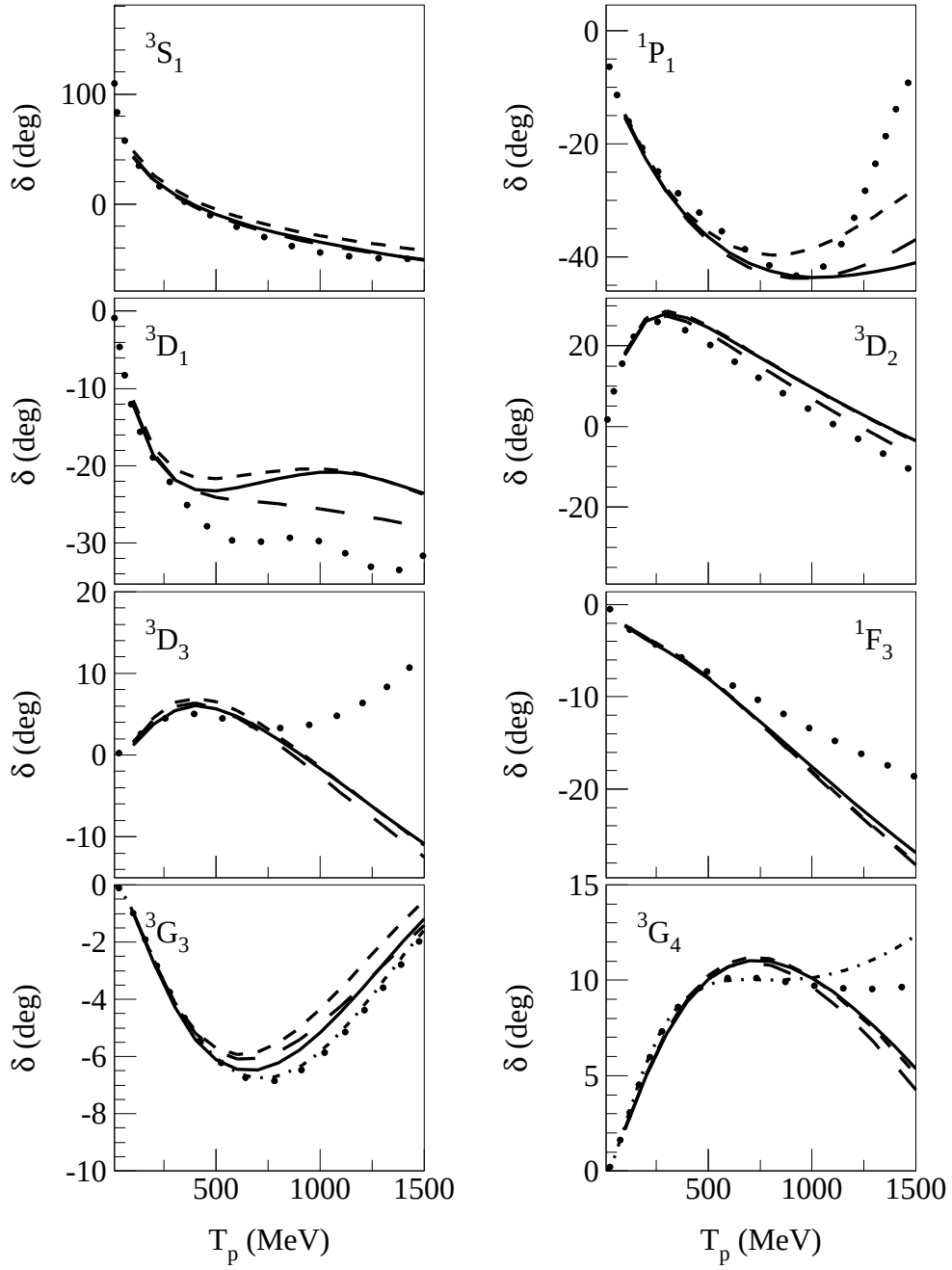

FIG. 16: The $T = 0$ NN partial wave phase shifts up to J=4 as function of the projectile laboratory kinetic energy. The notation of the curves is the same as in Fig. 15.

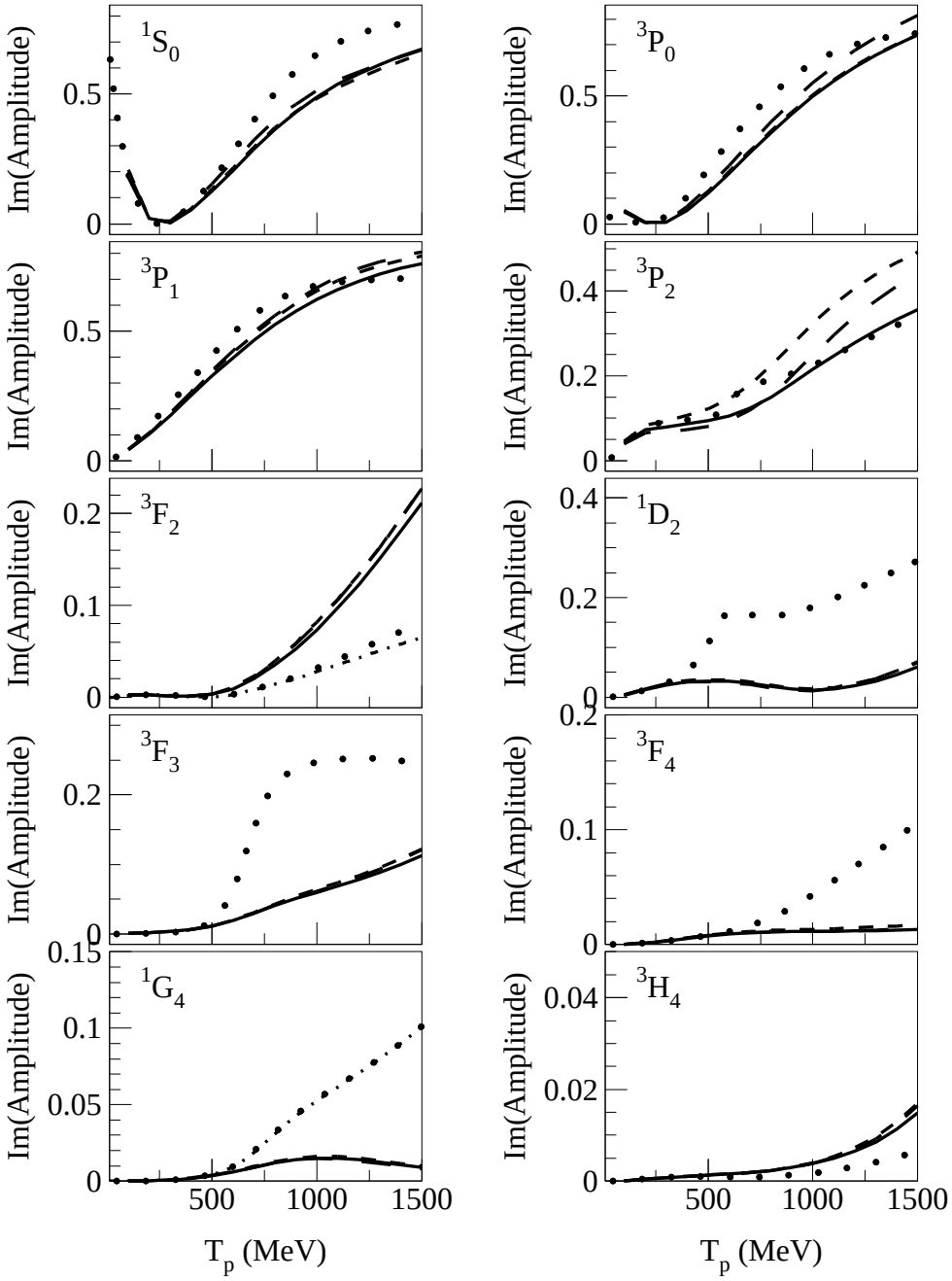

FIG. 17: The imaginary parts of the $T = 1$ NN partial wave amplitudes up to J=4 as function of the projectile laboratory kinetic energy. The notation of the curves is the same as in Fig. 15.

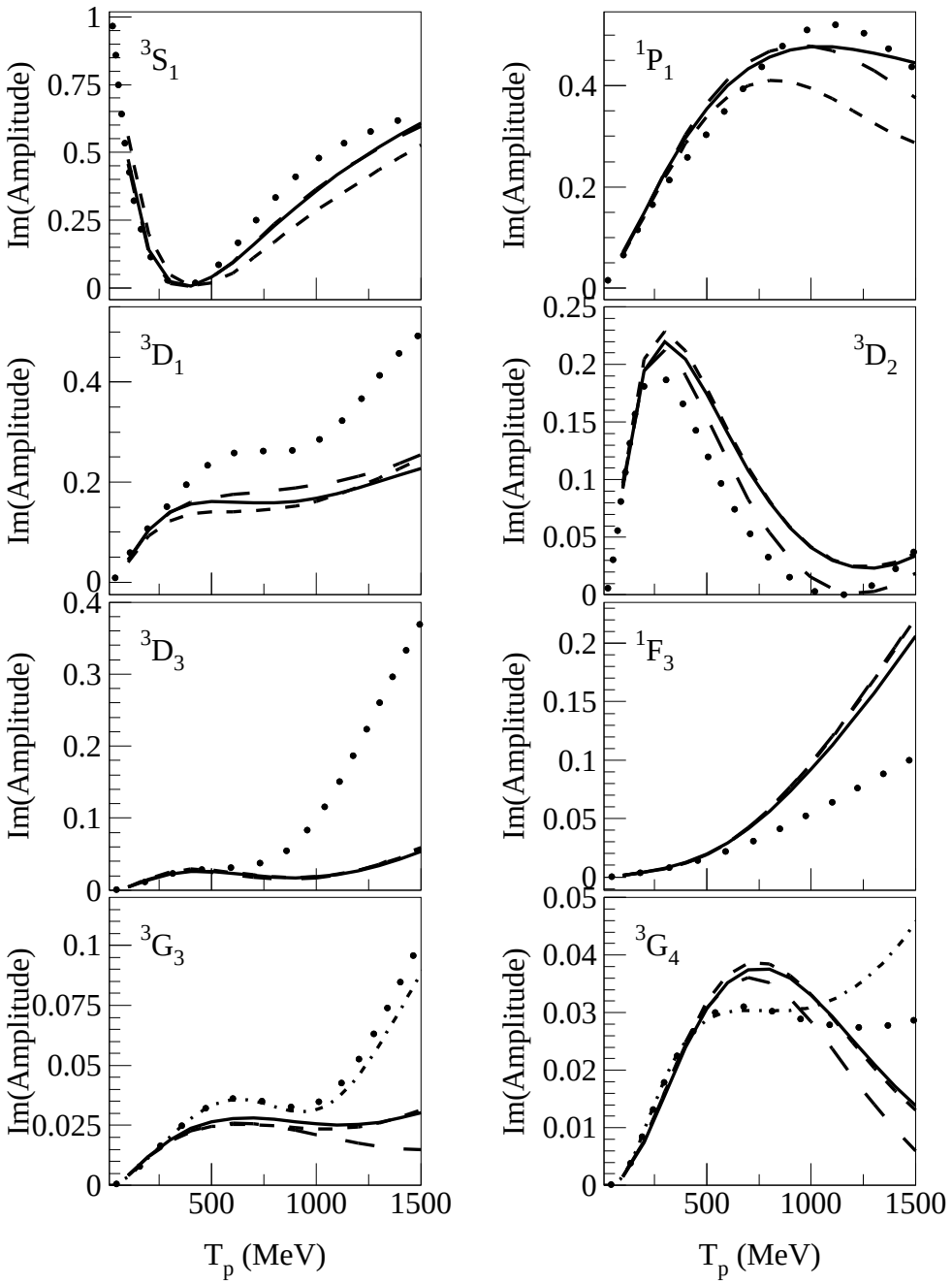

FIG. 18: The imaginary parts of the $T = 0$ NN partial wave amplitudes up to J=4 as function of the projectile laboratory kinetic energy. The notation of the curves is the same as in Fig. 15.

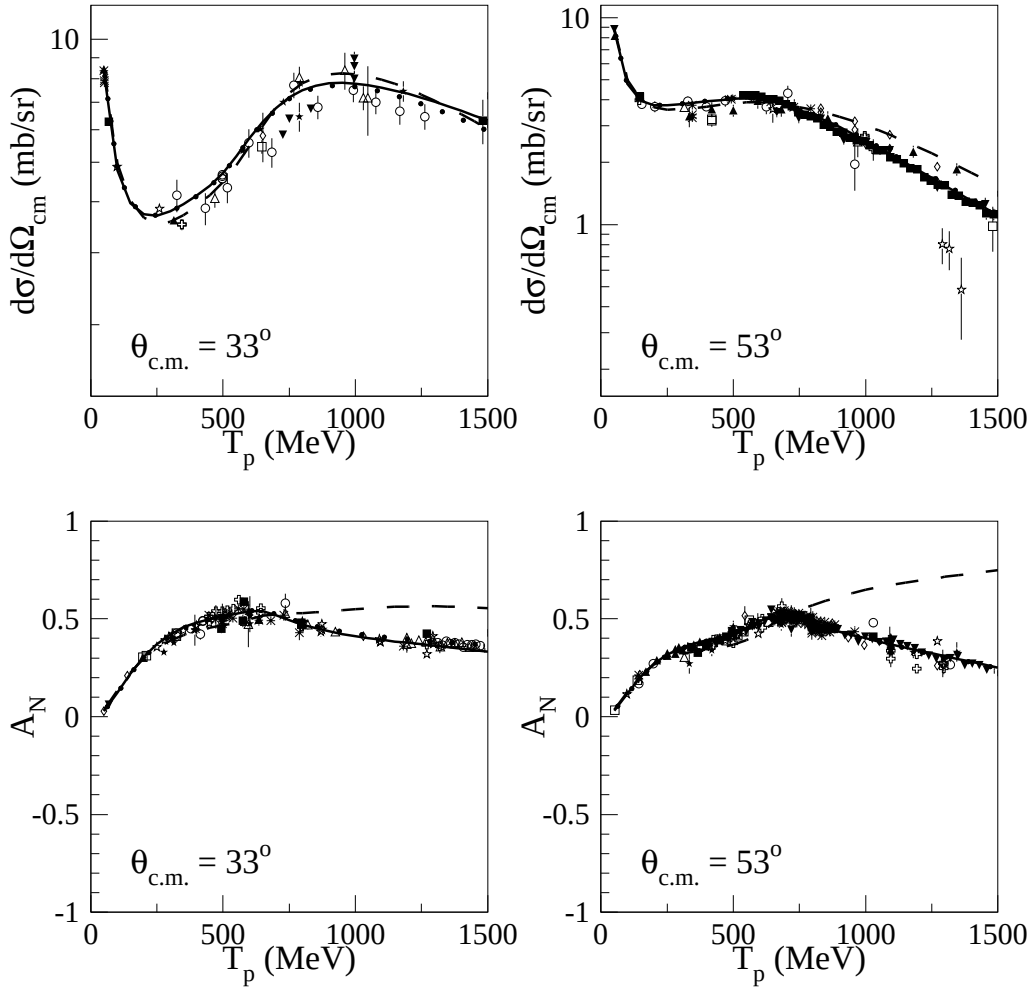

FIG. 19: The differential cross section (top panels) and the analyzing power A_N (bottom panels) for *pp* scattering as function of the laboratory projectile kinetic energy at two selected angles. The dashed lines are based on the calculation with the parameters of our model A (Table III). For the solid line the $^3P_2$ phase shift of the model is replaced by the SAID analysis. The experimental data are referenced in the SAID database [4].

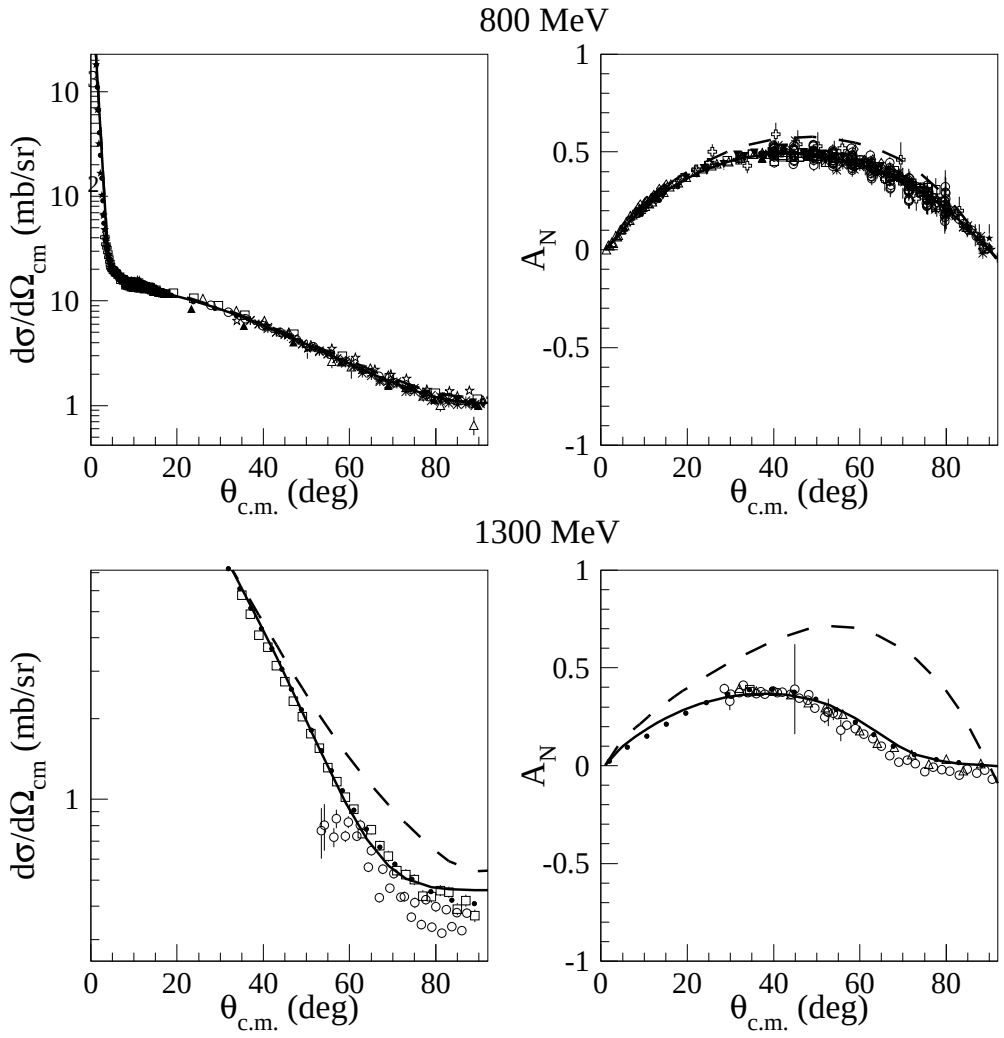

FIG. 20: The angular distribution of the differential cross section (left panels) and the analyzing power for *pp* scattering at 800 MeV laboratory kinetic energy (top panels) and 1300 MeV (bottom panels). The notation of the curves is the same as in Fig. 19. The experimental data are referenced in the SAID database [4].